Geoscience Frontiers 7 (2016) 743–757

HOSTED BY

Contents lists available at ScienceDirect

China University of Geosciences (Beijing)

Geoscience Frontiers

journal homepage: www.elsevier.com/locate/gsf

Research paper

Geochemistry of the volcanic rocks from Bioko Island ("Cameroon Hot Line"): Evidence for plume-lithosphere interaction

Fadimatou Ngounouno Yamgouot [a,*], Bernard Déruelle [b], Isaac Bertrand Gbambié Mbowou [c], Ismaïla Ngounouno [c], Daniel Demaiffe [d]

[a] Département des Sciences de la Terre, Faculté des Sciences, Université de Ngaoundéré, B.P. 454, Ngaoundéré, Cameroon
[b] Laboratoire de Magmatologie et Géochimie Inorganique et Expérimentale (MAGIE), Institut de Physique du Globe de Paris, UMR 7154, Université Pierre et Marie Curie, 4, place Jussieu, 75252, Paris cédex 05, France
[c] Département des Mines et de la Géologie, Ecole de Géologie et d'Exploitation Minière (EGEM), Université de Ngaoundéré, B.P. 115, Meiganga, Cameroon
[d] Laboratoire de Géochimie Isotopique et Géodynamique Chimique, DSTE, (CP 160/02) Université Libre de Bruxelles 50, av. Roosevelt, 1050, Bruxelles, Belgium

ARTICLE INFO

Article history:
Received 9 June 2014
Received in revised form
28 April 2015
Accepted 1 June 2015
Available online 9 July 2015

Keywords:
Geochemistry
HIMU-EM1
Volcanic rocks
Bioko
Cameroon Hot Line

ABSTRACT

Bioko Island (3008 m a.s.l) is located in the presently more active volcanic zone of the Cameroon Line and composed essentially of alkaline basalts and hawaiites, and lesser mugearites. The rocks show microlitic porphyritic texture with phenocrysts of olivine (83% < Fo < 87%) and clinopyroxene in a matrix of plagioclase, clinopyroxene and oxides. Hawaiites and mugearites also include phenocrysts of plagioclase ($An_{62-67}Ab_{35-32}Or_{3-1}$). Major element variation diagrams show an increase in SiO_2, Al_2O_3, Na_2O and K_2O with increasing MgO for the studied rock groups. The rocks are characterized by low $(^{86}Sr/^{87}Sr)_i$ ratios (0.70320–0.70406), high $\varepsilon_{Nd}(t)$ values (2.56–4.33) and high $(^{206}Pb/^{204}Pb)_i$ ratios (20.032–20.035) values. Basalts are enriched in LILE and LREE, and have $(Hf/Sm)_N = 0.57–1.16$. These geochemical signatures are similar to those of the Mount Cameroon rocks, and might be attributed to low degrees of partial melting from a garnet-amphibole-bearing mantle source. The trace elements and isotopic compositions suggest that the parental magma source might have involved HIMU- and EM1-components.

1. Introduction

Bioko Island (formerly called Fernando Poo) is located in the gulf of Guinea, the oceanic sector of the Cameroon Hot Line (CHL, inset Fig. 1), at about 35 km to the SW of the Mount Cameroon (continental sector). This Island is composed mainly of three young (<1.33 ± 0.07 Ma; K/Ar dating on basalt; Hedberg, 1969; Aka et al., 2004; Chauvel et al., 2005) strato-volcanoes (Fig. 1): Pico Santa Isabel, Pico Biao, and San Carlos. The ages of these volcanoes are more or less similar to those of Mount Cameroon (Déruelle et al., 1987). Indeed, Cameroon Hot Line (CHL) is a N30°E alignment of oceanic and continental volcanoes, and anorogenic units, extending from Pagalu Island in Gulf of Guinea to Lake Chad (Déruelle et al., 1991; Ngounouno et al., 2006; Déruelle et al., 2007; Mbowou et al., 2012). According to Déruelle et al. (2007), the geochemical and isotopic similarities between the oceanic and continental basalts attest that the continental crust did not play any role in the magma genesis and that the source is not of lithospheric origin. The oceanic sector of the Cameroon Hot Line is built upon a young oceanic lithosphere of upper Cretaceous age, while the continental lithosphere is much older and of Pan-African age (>500 Ma). Thus, to precise the nature of this mantle source, the detailed geochemical study of Bioko rocks, which are located in the transitional zone between the continent and ocean, is necessary. However, this work could be considered as a part of the debate on the origin of magmas in the ocean–continental transitional zone. The petrological and geochemical study of the Bioko Island volcanic rocks would clarify the nature of the magmatic sources in comparison with the other rocks from CHL.

This paper adds to an earlier paper on the petrology of Bioko Island volcanic rocks (Yamgouot et al., 2015) by presenting new and detailed geochemical and isotopic data, and evaluating the petrogenesis of these rocks. Our data provide evidence for fractional

* Corresponding author.
E-mail address: yamgouotfadimatou@yahoo.fr (F.N. Yamgouot).
Peer-review under responsibility of China University of Geosciences (Beijing).

http://dx.doi.org/10.1016/j.gsf.2015.06.003

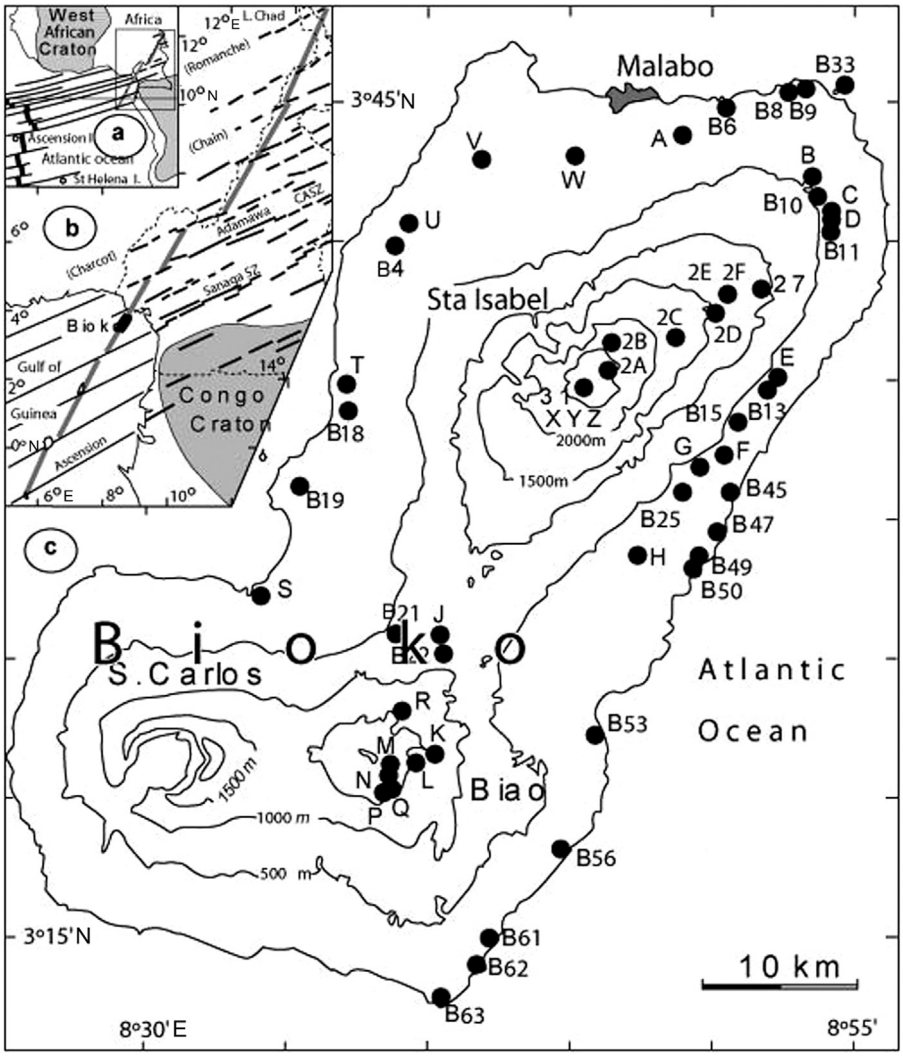

Figure 1. (a) The Cameroon Hot Line trends N30°E (thick grey lines). Its continental sector is segmented by Pan-African shear zones in Africa propagating as fracture zones into the Atlantic Ocean (data after Fail et al., 1970; Meyers et al., 1998; Déruelle et al., 2007 and the references therein). Its northern extension towards Lake Chad is tentative. (b) Schematic geological map of the Guinea Gulf showing the outcrop of the Cameroon line volcanic rocks (black), modified after Halliday et al. (1995). The continuous line represents the major oceanic transform faults after Sibuet and Mascle (1978); the dashed lines delimit the continental zone (CZ), the transitional zone (TZ) and the oceanic zone (OZ) after Fitton (1987); the dotted lines in the Congo craton correspond to Proterozoic dykes of doleritic composition. (c) Location map of the mean centre of the Bioko volcanic island, including sample locations on Bioko Island.

crystallization, as well as the role of partial melting process. We also attempt to characterize the mantle source rocks.

2. Geological setting

Bioko Island (GPS coordinates: 8°20′–8°55′E; 3°10′–3°50′N), is the largest (700 km^2) of the four islands of the Gulf of Guinea. It is located in the southern part of the CHL in the ocean–continent transitional zone. The Bioko Island is composed of numerous fresh pyroclastic cones, which testify likely of recent volcanic activities. Although, the recorded eruptions of 1898, 1903 (Enciclopedia Universal, 1924) and 1923 (Déruelle et al., 1987) are known. Pico Santa Isabel in the northern part culminates at 3008 m a.s.l. Pico Biao, the smallest, culminates at 2009 m a.s.l. in the South-East part, and has a small crater lake (diameter: 0.4 km). Its southeastern and southwestern flanks are bordered by N30°E and N130°E faults which give a rectilinear aspect from the shore. San Carlos located in the South-West of the island, is characterized by the presence of a caldera (diameter: 6 km). It is composed of cinder cones which gives it a regular shape. More geological descriptions on the Bioko Island volcanoes are presented by the following author (Boëse, 1912). Two types of volcanic products were found on the Bioko Island: pyroclastic ejection (spheroid bombs, cognate blocks, lapilli, coarse and fine ash, and shiny and black scoriae) and rock flows. The majority of eruptions produced on the Bioko Island are typically strombolian. Vents are often more or less opened fractures, and many of them can be simultaneously active. Explosive vents are mild, with average projected amount to 300–400 m high. A paroxysmal phase is followed by a sustained long activity. The main cone reaches a few tens of meters in height, with an outer slope of about 30°. Cones built partly of effusive and partly of pyroclastic layers have long been referred to as stratovolcanoes.

All are also not visible or are destroyed and indistinguishable from other cinder newer cones or from cones hidden by the vegetation for those located below the limit of the forest. Hundred maars were described on the Bioko Island. These phreatomagmatic eruptions are originally low rimmed tuff rings, cone composed of a lowered accumulation ejecta and block levels. The pyroclastic ejecta are often muddy and hot for a strong cementing pyroclastic. Maars are located in the summit area and on the flanks of the stratovolcanoes. They

result from the accumulation of bombs and lapilli around the vent. The scoriae can be uncemented (strombolian cone) or heat sealed (spatter-cone) and may be complete or with the neck broken, more often, especially on slopes. It may be noted that multiple vents formed in the same eruptive cycle, have the highest summits rich in pyroclastics because most of the degassing occurs there, while the lowest are more effusive producing more rock. This is well illustrated by the eruption of 1903 which formed a crater explosion and a lot of ash 3000 m above sea level, a cinder cone and a small rock flow at 2400 m. In the most common cases, flows tend to flow to low levels at the base of the volcanoes when they find access at the intersection of a secondary fracture. Much more widespread, these rock flows are characterized by smooth, billowing, ropy, or entrail-like crusts of quenched glass formed of blocks of basalts of all sizes mainly accumulated on the flanks of the rock flows. On gently sloping plateaus, the rock flows spread in large sheets on which only cones emerge. On moderate to steep slopes, when leaving plateaus, the velocity of the flow core increases.

3. Sampling and analytical methods

Thin sections were prepared for all samples. Electron microprobe analyses of mineral phases (olivine, clinopyroxene, feldspar, Fe–Ti oxides and amphibole) were performed in polished thin sections using CAMEBAX SX50 and SX100 at Université Pierre-et-Marie Curie, Paris. The measurements were made according to standard analyzed data, under the conditions expressed in kV (accelerating voltage), nA (beam current) and s (counting times at the peak). Olivine (15 kV, 40 nA, 20 s for all elements, except Si (10 s)), clinopyroxene (15 kV, 40 nA, 20 s for Si, Al, Fe, Mg, Ca, Na, Mn and 30 s for Ti and Zr), feldspar (15 kV, 10 nA, 5 s for all elements), Fe–Ti oxides (15 kV, 40 nA, 40 s for Ti, Fe, Mn, Mg; 10 s for Si, 15 s for Cr and 30 s for Al), amphibole (15 kV, 10 nA, 15 s for Si, Al, Mg, Na and K, 20 s for Ca and Ti, 25 s for Fe and Mn, 30 s for Cl and F). Measurements correction was carried out using the "PAP" program (Pouchou and Pichoir, 1991). Analyses are given in terms of oxides of the elements (wt.%).

Whole-rock chemical analyses of basaltic rocks from Bioko Island were carried out at CRPG laboratory, Nancy (France). Major elements (46 samples) were analyzed by ICP-AES and trace elements (23 samples) by ICP-MS. The samples were previously selected in order to limit superficial contamination, then crushed. Details of other analytical processes were presented elsewhere (Carignan et al., 2001). Samples for Sr and Nd isotopic analyses were dissolved in mixed $HF–HNO_3$ (10:1) acid mixture; chemical separation was carried out by cation exchange chromatography; blanks were<1 ng. Sr and Nd isotopic ratios were measured on a VG Sector 54 multicollector thermal ionisation mass spectrometer (Université Libre de Bruxelles). Replicate analyses of the MERCK Nd standard gave an average $^{143}Nd/^{144}Nd$ value of 0.5127428 (normalized to $^{143}Nd/^{144}Nd = 0.7219$), and measurements of NBS 987 Sr yielded an average $^{87}Sr/^{86}Sr$ value of 0.710247 (normalized to $^{86}Sr/^{88}Sr = 0.1194$). ε_{Nd} values were calculated assuming $^{147}Sm/^{144}Nd = 0.1967$ and $^{143}Nd/^{144}Nd = 0.512638$ for CHUR (see Ashwal et al. (2002) for a detailed description of the procedure). CIPW-normative compositions were calculated on a water-free basis with $Fe_2O_3/FeO = 0.2$ for basalt and 0.3 for hawaiite according to Middlemost (1975).

4. Results

4.1. Field characteristics and petrography

The samples are mainly sampled from the North and East of the Bioko Island. The access to the Southeast sector of the volcano is difficult because of forest cover and intense rain fall, well preserved

Table 1
Representative chemical analyses of olivine from Bioko Island volcanic rocks.

Rock type	Basalt															Hawaiite			
Sample	L	L	1A	1A	B	B	D	D	J	J	Q	Q	W	W	2E	2E	2E	F	F
Description	ph.c	ph.r	ph.c	ph.r	ph.c	ph.r	ph.c	ph.r	ph.c	ph.r	ph.c	ph.r	ph.c	ph.r	ph.c	ph.r	m	ph.c	ph.r
SiO_2 (wt.%)	40.44	39.87	39.59	39.79	40.23	38.83	39.92	39.42	39.60	38.69	37.62	37.77	40.27	39.86	40.14	39.57	39.71	40.60	39.12
TiO_2	0.04	0.01	0.00	0.06	0.02	0.04	0.02	0.06	0.03	0.06	0.05	0.06	0.02	0.00	0.02	0.04	0.04	0.05	0.06
Al_2O_3	0.04	0.03	0.02	0.01	0.02	0.01	0.03	0.04	0.03	0.03	0.04	0.03	0.01	0.04	0.05	0.01	0.02	0.02	0.02
FeO	12.54	15.76	16.72	16.22	13.65	20.70	16.21	16.07	15.74	20.74	27.08	27.12	15.45	15.35	15.20	15.10	15.20	13.15	21.03
MnO	0.09	0.23	0.25	0.17	0.07	0.37	0.16	0.26	0.25	0.27	0.54	0.40	0.18	0.14	0.19	0.21	0.17	0.19	0.28
MgO	46.20	43.95	42.86	43.55	45.48	39.34	43.47	43.68	43.16	39.18	34.08	34.66	44.03	44.36	44.24	42.93	43.92	46.02	39.47
CaO	0.22	0.23	0.18	0.32	0.21	0.39	0.26	0.22	0.28	0.43	0.41	0.42	0.34	0.34	0.16	0.22	0.23	0.18	0.32
NiO	0.32	0.19	0.16	0.20	0.30	0.18	0.25	0.22	0.13	0.11	0.10	0.13	0.27	0.18	0.36	0.28	0.29	0.30	0.10
Total	99.90	100.28	99.77	100.32	99.99	99.85	100.31	99.97	99.23	99.50	99.92	100.58	100.55	100.26	100.36	98.36	99.58	100.50	100.40
Si (a.p.f.u)	2.010	2.005	2.009	2.004	2.008	2.010	2.010	1.994	2.012	2.009	2.009	2.002	2.015	2.001	2.011	2.023	2.006	2.011	2.013
Ti	0.001	0.000	0.000	0.002	0.001	0.001	0.001	0.002	0.001	0.002	0.002	0.002	0.001	0.000	0.001	0.001	0.001	0.002	0.002
Fe	0.521	0.663	0.710	0.683	0.570	0.896	0.683	0.680	0.669	0.901	1.210	1.202	0.647	0.644	0.637	0.646	0.642	0.545	0.905
Mn	0.004	0.010	0.011	0.007	0.003	0.016	0.007	0.011	0.011	0.012	0.025	0.018	0.008	0.006	0.008	0.009	0.007	0.008	0.012
Mg	3.424	3.294	3.243	3.270	3.384	3.036	3.263	3.293	3.270	3.033	2.713	2.739	3.285	3.319	3.304	3.272	3.308	3.398	3.028
Ca	0.012	0.013	0.010	0.017	0.011	0.021	0.014	0.012	0.015	0.024	0.024	0.024	0.018	0.018	0.009	0.012	0.012	0.009	0.018
Ni	0.013	0.008	0.006	0.008	0.012	0.007	0.010	0.009	0.005	0.005	0.004	0.006	0.011	0.007	0.015	0.012	0.012	0.012	0.004
Mg#	0.87	0.83	0.82	0.83	0.86	0.77	0.83	0.83	0.83	0.77	0.69	0.69	0.84	0.84	0.84	0.84	0.84	0.86	0.77
Fa	0.13	0.17	0.18	0.17	0.14	0.23	0.17	0.17	0.17	0.23	0.31	0.30	0.16	0.16	0.16	0.16	0.16	0.14	0.23
Fo	0.87	0.83	0.82	0.82	0.85	0.77	0.82	0.83	0.83	0.77	0.69	0.69	0.83	0.83	0.84	0.83	0.83	0.86	0.77

ph = phenocryst, c = core, r = rim, m = microlite.

Table 2
Representative chemical analyses of clinopyroxene from Bioko Island volcanic rocks.

Rock type	Basalt														Hawaiite		Mugearite	
Sample	L	L	L	A	D	D	D	J	J	W	W	W	2E	2E	F	Z	F	G
Description	ph.c	ph.b	ph	ph.c	ph.c	ph.b	ph	ph.c	ph.b	ph.c	ph.b	ph	ph.c	ph.b	ph.c	ph.c	ph	ph.c
SiO_2 (wt.%)	48.65	50.82	51.23	49.47	51.01	51.82	49.16	47.23	40.36	47.59	48.61	46.76	49.81	48.89	47.64	49.07	50.02	50.04
TiO_2	1.523	1.171	0.967	1.736	1.299	1.007	1.67	2.492	5.743	2.465	2.06	2.667	1.726	2.227	2.852	2.147	1.633	1.943
Al_2O_3	7.552	2.955	3.38	4.372	3.042	3.148	5.162	5.787	11.24	5.887	4.78	6.556	3.947	5.177	6.282	4.185	4.312	3.966
FeO	6.566	5.555	4.691	7.329	6.387	5.991	6.268	7.733	8.707	7.405	6.879	7.254	6.043	6.751	7.082	6.838	5.834	7.54
MnO	0.034	0.098	0.068	0.23	0.142	0.145	0.025	0.084	0.09	0.102	0.096	0.127	0.07	0.196	0.187	0.16	0.005	0.238
MgO	13.95	15.57	15.53	13.11	15.53	15.61	13.86	13.41	9.998	13.46	14.07	12.85	14.74	14.08	12.94	13.81	14.43	13.79
CaO	20.13	22.49	22.47	22.5	21.79	20.72	22.37	22.23	22.42	22.25	22.38	21.85	21.66	21.45	22.59	22.11	23.07	21.7
Total	98.41	98.66	98.34	98.75	99.2	98.45	98.51	98.96	98.56	99.17	98.87	98.06	98	98.77	99.57	98.33	99.3	99.22
Si (a.p.f.u)	1.807	1.894	1.904	1.858	1.894	1.924	1.840	1.782	1.552	1.785	1.824	1.772	1.870	1.827	1.778	1.848	1.857	1.866
Ti	0.043	0.033	0.027	0.049	0.036	0.028	0.047	0.071	0.166	0.070	0.058	0.076	0.049	0.063	0.080	0.061	0.046	0.055
Al	0.331	0.130	0.148	0.194	0.133	0.138	0.228	0.257	0.509	0.260	0.211	0.293	0.175	0.228	0.276	0.186	0.189	0.174
Al^{VI}	0.193	0.106	0.096	0.142	0.106	0.076	0.160	0.218	0.448	0.215	0.176	0.228	0.130	0.173	0.222	0.152	0.143	0.134
Al^{IV}	0.137	0.024	0.052	0.052	0.027	0.061	0.068	0.039	0.061	0.046	0.035	0.065	0.044	0.055	0.054	0.034	0.046	0.041
Fe	0.204	0.173	0.146	0.230	0.198	0.186	0.196	0.244	0.280	0.232	0.216	0.230	0.190	0.211	0.221	0.215	0.181	0.235
Fe^{3+}	0.000	0.000	0.000	0.000	0.000	0.000	0.000	0.000	0.000	0.000	0.000	0.000	0.000	0.000	0.000	0.000	0.000	0.000
Fe^{2+}	0.204	0.173	0.146	0.230	0.198	0.186	0.196	0.244	0.280	0.232	0.216	0.230	0.190	0.211	0.221	0.215	0.181	0.235
Mn	0.001	0.003	0.002	0.007	0.004	0.005	0.001	0.003	0.003	0.003	0.003	0.004	0.002	0.006	0.006	0.005	0.000	0.008
Mg	0.772	0.865	0.860	0.734	0.859	0.864	0.773	0.754	0.573	0.753	0.787	0.726	0.824	0.784	0.720	0.775	0.799	0.766
Ca	0.801	0.898	0.895	0.906	0.867	0.824	0.897	0.898	0.923	0.894	0.900	0.887	0.871	0.859	0.903	0.892	0.918	0.867
Na	0.055	0.022	0.024	0.034	0.022	0.023	0.033	0.021	0.043	0.034	0.028	0.038	0.029	0.035	0.038	0.031	0.028	0.042
mg#	0.79	0.83	0.86	0.76	0.81	0.82	0.80	0.76	0.67	0.76	0.78	0.76	0.81	0.79	0.77	0.78	0.82	0.77
En	0.52	0.48	0.50	0.43	0.48	0.49	0.47	0.45	0.42	0.44	0.45	0.45	0.48	0.48	0.45	0.45	0.47	0.44
Wo	0.36	0.44	0.43	0.44	0.43	0.39	0.43	0.44	0.45	0.46	0.46	0.44	0.42	0.41	0.44	0.44	0.45	0.43
Fs	0.12	0.08	0.08	0.12	0.09	0.12	0.10	0.11	0.13	0.10	0.09	0.11	0.10	0.11	0.11	0.11	0.09	0.12

ph = phenocryst, c = core, r = rim, m = microlite.

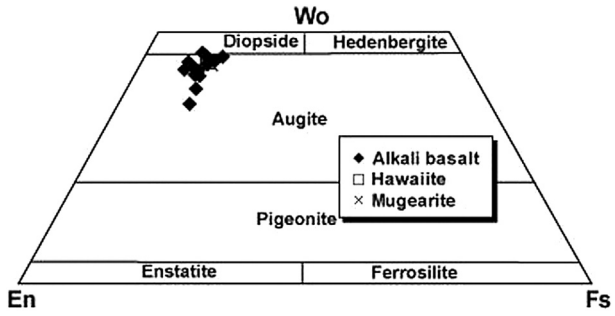

Figure 2. Compositional variations of clinopyroxene phenocrysts and microlites from the Bioko Island volcanic rocks in the Wo–En–Fs ternary diagram (Morimoto, 1989) for basaltic rocks from Bioko island.

craters, including the summit of the island and the presence of shiny and black scoriae confirm the youth of these formations. Basaltic rocks (Yamgouot et al., 2015) have been found in the Bioko Island. Basaltic rocks only have been sampled on the neighbouring continental Mount Cameroon volcano (Déruelle et al., 1987).

All the Bioko Island volcanic rocks are porphyric often vacuolar and contain partly altered olivine and clinoproxene phenocryts. On the basis of their mineral composition, the Bioko Island volcanic rocks can be subdivided into basalt, hawaiite and mugearite.

Basalts show porphyric microlitic texture and are composed of olivine (0.5–2.0 mm; 10–20 vol.%), clinopyroxene (0.2–5.0 mm; 5–15 vol.%) and Fe–Ti oxides (<2 vol.%) phenocrysts. The groundmass is fine-grained with intergranular to intersertal texture, and is composed of plagioclase laths, subhedral to anhedral brown clinopyroxene and Fe–Ti oxides.

Some olivine crystals are skeletal; likely derived from the fast cooling of the ejected lavas.

Hawaiites contain plagioclase phenocrysts, subordinate olivine phenocrysts and strongly zoned clinopyroxene phenocrysts with pink core and brownish rim in a fine-grained groundmass rich in plagioclase, granular clinopyroxene and opaque oxides microlites. One sample (K) contains microphenocrysts of amphibole.

Mugearites are present and characterized by a subaphyric microlitic texture with 5% of euhedral olivine, pyroxene and plagioclase phenocrysts. The groundmass is composed of glass (50 vol.%), microlites of plagioclase (50–20 μm), microcrysts of pyroxene and Fe–Ti oxides.

Table 3
Representative chemical analyses of Fe-Ti oxides from Bioko Island volcanic rocks.

Rock type	Basalt		Hawaiite		
Sample	W	W	S	S	S
SiO_2 (wt.%)	0.09	0.06	0.12	0.08	0.09
TiO_2	23.38	45.96	16.71	14.83	17.17
Cr_2O_3	0.15	0.00	0.01	0.01	0.04
Al_2O_3	1.52	0.01	4.01	5.31	4.83
FeO	66.64	44.39	66.01	68.32	67.35
MnO	0.82	0.96	0.84	0.64	0.81
MgO	2.01	2.25	4.04	4.76	4.83
CaO	0.13	0.15	0.17	0.05	0.06
Na_2O	0.02	0.04	0.04	0.01	0.03
NiO	0.04	0.00	0.00	0.05	0.00
Total	94.78	93.83	91.94	94.06	95.20
Si (a.p.f.u.)	0.003	0.002	0.004	0.003	0.003
Ti	0.540	0.936	0.398	0.346	0.392
Cr	0.004	0.000	0.000	0.000	0.001
Al	0.055	0.000	0.150	0.194	0.173
Fe	1.710	1.005	1.749	1.772	1.709
Mn	0.021	0.022	0.022	0.017	0.021
Mg	0.092	0.091	0.191	0.220	0.218
Ca	0.004	0.004	0.006	0.002	0.002
Na	0.001	0.002	0.002	0.000	0.002
Ni	1.390	0.000	0.000	1.783	0.000

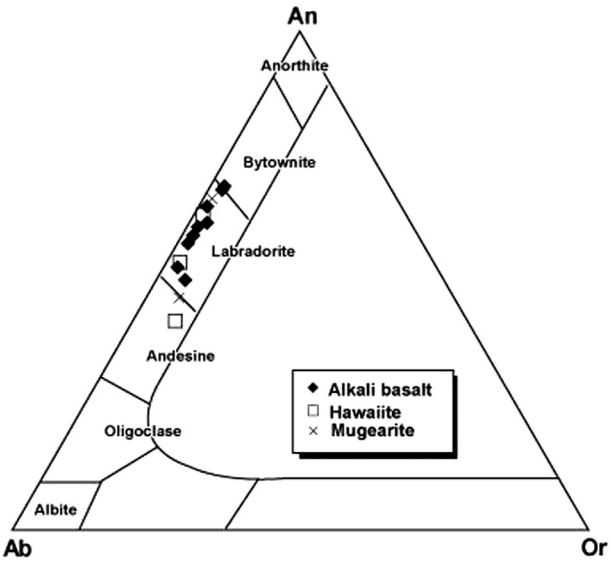

Figure 3. Compositional variations of the plagioclase phenocrysts and microlites from the Bioko Island volcanic rocks in the An–Ab–Or diagram.

4.2. Mineral chemistry

4.2.1. Olivine

Mg-rich olivine phenocrysts (Table 1) occur in basalts ($Fo_{69–87}$) and hawaiites ($Fo_{86–77}$) from Bioko Island. In the basalts and hawaiites, the phenocrysts are usually unzoned. The low CaO content (<0.5 wt.%) in these phenocrysts results probably from high-pressure crystallization (~0.2 GPa). Crystallization temperatures for olivine phenocrysts have been estimated at 1150 ± 20 °C (after Roeder and Emslie, 1970; Leeman, 1978; using whole rock composition as a liquid).

4.2.2. Clinopyroxene

Ca-rich pyroxene phenocrysts occur in alkali basalts, hawaiites and mugearites (Table 2). Compositions range from $Wo_{36}En_{52}Fs_{12}$ to $Wo_{45}En_{42}Fs_{13}$ and plot mainly to augite field, with high $Mg^{\#} = [Mg/(Mg + Fe^{2+})]$ values (0.67–0.87). Some compositions straddle the boundary of diopside and augite fields (see Fig. 2). Furthermore, TiO_2 contents were high in few diopside (up to 5.7 wt.%) and augite (up to 2.9 wt.%) phenocrysts. The crystallization pressure of the clinopyroxene was estimated using the structural barometer of Marsh (1988) and Nimis and Ulmer (1998). This geobarometer for basaltic system was calibrated on the basis of unit cell and M1 volumes. For this purpose, structure parameters were estimated starting from the chemical compositions of several C2/c pyroxene crystals produced in high-pressure experimental runs. Thus, it is suitable for anhydrous system. The results are: (1) the small phenocrysts of Ti-augite composition were equilibrated at low pressure (<0.2 GPa); while (2) the few larger ones (diopside composition) crystallized at significantly higher pressure (~0.6 GPa). In few samples, the clinopyroxene phenocrysts are zoned: the diopside cores crystallized at high pressure and the Ti-augite rims at low pressure. Pressure estimated suggests probably a polybaric crystallization of Bioko basaltic magma. Similar multi-chamber evolution is common in alkaline (Woodland and Jugo, 2007) and peralkaline (Berger et al., 2008) volcanic rocks.

Table 4
Representative chemical analyses of plagioclase from Bioko Island volcanic rocks.

Rock type	Basalt										Hawaiite			Mugearite	
Sample	L	B	D	D	J	Q	J	W	W	Z	F	F	S	G	G
Description	ph.c	ph.c	ph.c	ph	ph	m	ph.c	ph.c	ph	ph.c	ph.c	ph	ph	ph	ph
SiO_2 (wt.%)	51.34	53.07	53.50	59.95	50.40	52.99	50.85	54.91	52.44	55.35	52.18	54.64	56.36	57.79	51.40
Al_2O_3	30.20	28.98	29.31	24.75	31.11	29.92	31.28	28.77	29.98	27.37	30.22	28.90	26.65	25.95	30.86
FeO	0.65	0.68	0.84	0.72	0.68	0.60	0.85	0.57	0.87	0.63	0.78	0.83	1.33	0.95	0.77
Na_2O	3.85	4.58	4.55	6.95	3.21	4.05	3.34	5.08	4.22	5.26	4.07	5.03	5.94	5.31	3.65
K_2O	0.21	0.29	0.30	1.89	0.38	0.52	0.39	0.41	0.33	0.85	0.26	0.40	1.29	0.94	0.25
CaO	13.36	11.69	12.34	5.69	13.89	12.66	13.87	10.72	12.39	10.58	13.05	11.05	8.83	9.30	13.64
Total	99.61	99.29	100.83	99.94	99.67	100.74	100.58	100.46	100.23	100.05	100.54	100.85	100.41	100.24	100.57
Si (a.p.f.u)	2.350	2.425	2.413	2.690	2.309	2.392	2.311	2.470	2.381	2.507	2.365	2.455	2.548	2.598	2.332
Al	1.629	1.561	1.558	1.309	1.680	1.592	1.675	1.525	1.604	1.461	1.614	1.531	1.420	1.375	1.650
Fe	0.025	0.026	0.032	0.027	0.026	0.023	0.032	0.021	0.033	0.024	0.030	0.031	0.050	0.036	0.029
Ca	0.655	0.572	0.596	0.274	0.682	0.612	0.675	0.517	0.603	0.514	0.634	0.532	0.428	0.448	0.663
Na	0.342	0.405	0.398	0.604	0.286	0.354	0.294	0.443	0.372	0.462	0.358	0.438	0.520	0.462	0.321
K	0.012	0.017	0.017	0.108	0.022	0.030	0.022	0.024	0.019	0.049	0.015	0.023	0.075	0.054	0.015
Ab (%)	33.88	40.76	39.36	61.30	28.85	35.56	29.65	45.03	37.43	45.09	35.55	44.11	50.89	47.95	32.12
Or	1.24	1.68	1.68	10.95	2.26	3.00	2.25	2.41	1.89	4.81	1.47	2.31	7.29	5.61	1.46
An	64.88	57.56	58.96	27.75	68.89	61.44	68.10	52.56	60.68	50.10	62.99	53.58	41.82	46.44	66.42

ph = phenocryst, c = core, m = microlite.

4.2.3. Fe–Ti oxides

In basalts, magnetite and ilmenite have been analyzed (Table 3). Hawaiites contain only magnetite, with FeO and TiO_2 contents reaching 68.3 wt.% and 17.2 wt.% respectively. The equilibrium temperatures comprised between 950 °C and 1000 °C (±20 °C) were established for the ilmenite-magnetite stability in Bioko Island basalts (estimated according to Spencer and Lindsey, 1981)

4.2.4. Plagioclase

Plagioclase phenocrysts compositions of basalts plotted in An-Ab-Or diagram, correspond to bytownite and labradorite fields (Fig. 3). Hawaiites contain labradorite and andesine, with FeO contents, which range from 0.7 wt.% to 13 wt.% (Table 4). Andesine is present in mugearite.

Table 5
Representative chemical analyses of amphibole from Hawaites from Bioko Island volcanic rocks.

Rock type	Hawaiite	mph.c
Sample	K	
Description	mph.c	
SiO_2 (wt.%)	38.28	38.9
TiO_2	6.15	5.98
Al_2O_3	12.6	12.88
Fe_2O_3	3.17	1.91
FeO	8.81	9.2
MnO	0.12	0.03
MgO	12.38	12.75
CaO	12.83	12.43
Na_2O	2.55	2.43
K_2O	1.31	1.25
Sum	98.25	97.76
Si (a.p.f.u)	5.69	5.78
Ti	0.69	0.67
Al	2.21	2.25
Fe^{3+}	0.36	0.21
Cr	0	0
Fe^{2+}	1.1	1.14
Mn	0.02	0.004
Mg	2.74	2.82
Ca	2.04	1.98
Na	0.73	0.7
Ni	0.01	0
K	0.25	0.24

mph = microphenocryts, c = core.

4.2.5. Amphibole

Ca-amphibole microphenocrysts (<0.5 mm) occur in hawaiite (K) (Table 5). These amphibole microphenocrysts with kaersutite characteristic (according to Leake et al., 1997) are TiO_2 rich mineral (TiO_2: up to 6.2 wt.%; Ti > 0.5 a.p.f.u). Kaersutite crystals have commonly been observed in evolved basaltic (hawaiite) rocks (Dautria et al., 1987).

4.3. Geochemistry

4.3.1. Whole-rock chemistry

Major and trace element compositions of Bioko Island volcanic rocks are given in Table 6. The samples are basalts, hawaiites and mugearites, according to Le Bas et al. (1986) diagram (Fig. 4). Apart from one sample which have high LOI (loss on ignition) values (2.5; sample N2), all the others rocks encountered in the Bioko Island have low LOI values (0.25–1.07) with moderate $Mg^{\#}$ (54–41; $Mg^{\#} = 100 \times [Mg/(Mg + Fe^{2+})]$, calculating with fixed $Fe_2O_3/FeO = 0.15$ ratio) indicative of an evolved magma. The whole-rock data indicate a regular compositional enrichment of SiO_2 contents from 42 wt.% to 54 wt.% (Table 6) and $Na_2O + K_2O$ from 1.6 to 7.4 wt.%. In the major oxides vs. MgO diagram (Fig. 5), Fe_2O_3 decreases with differentiation, MnO, TiO_2 and CaO are more constant, whereas Na_2O, SiO_2 and K_2O increase with differentiation, those variations are well correlated with petrographic observations (high MgO and Fe_2O_3 in basalts; low CaO variations illustrate the minor role of plagioclase at the beginning of the differentiation). The rocks have K_2O/Na_2O ratios of 0.21–0.74.

The Bioko Island volcanic rocks are poorer in SiO_2, Al_2O_3 and TiO_2 and richer in MgO than typical Oceanic Island Basalts (OIB) (McDonough and Sun, 1995), which is a common feature of oceanic intraplate basaltic volcanism. The trace element abundances of the Bioko Island volcanic rocks (Table 6) are typical of those of oceanic intraplate alkaline mafic magmas. Transitional elements illustrated by Ni and Cr (Fig. 6) are well correlated with Th; they are more enriched in alkali basalt (642–1883 ppm Cr and 268–784 ppm Ni), and hawaiites have relatively low Cr and Ni contents (79–12 ppm) and (387–10 ppm). The rocks (basalts and hawaiites) display a simple evolution line due to the fractionation of ol (±cpx) and cpx (±ol).

Table 6
Major and trace elements for Bioko Island volcanic rocks.

Rock type	Basalt																
Sample	N2	B53	B33	B8	L	N1	J	R	M	P	H	2E	Z	C	E	2C	
SiO_2 (wt.%)	42.62	44.46	49.3	42	43.77	42.3	42.55	41.79	44.67	46.11	42.65	43.95	44.2	44.85	43.9	42	
TiO_2	2.41	3.32	2.29	3.71	2.72	3.67	3.26	3.23	3.25	2.64	2.88	3.07	3.37	3	3.19	3.21	
Al_2O_3	10.65	10.05	14.41	11.66	11.46	11.62	13.77	16.18	12.74	12.82	12.25	11.13	12.4	12.81	13.16	11.87	
Fe_2O_3*	12.77	13.18	11.66	15.04	13.4	14.33	13.78	13.67	12.85	12.41	13.49	12.95	14.25	12.97	14.12	14.34	
MnO	0.2	0.19	0.15	0.18	0.21	0.18	0.19	0.24	0.19	0.19	0.18	0.17	0.18	0.19	0.18	0.19	
MgO	15.23	10.43	7.49	10.72	13.35	9.67	8.82	4.59	9.3	7.77	10.91	12.94	10.22	9.91	10.41	11.6	
CaO	11.42	13.12	10	11.44	11.05	12.18	11.57	9.84	11.44	11.68	10.84	9.92	10.61	10.93	10.09	10.83	
Na_2O	1.14	2.01	2.94	2.58	1.88	2.4	2.74	2.46	2.72	2.36	2.45	2.4	2.42	2.67	2.38	3.48	
K_2O	0.49	0.92	0.59	1.32	0.81	1.27	1.52	0.81	1.96	1.76	0.94	0.87	0.74	0.58	1.25	1.15	
P_2O_5	0.57	0.47	0.31	0.52	0.53	0.65	0.55	1.33	0.6	1.26	0.86	0.8	0.69	0.86	0.63	1.04	
LOI	2.53	0.37	0.35	0.1	1.07	0.25	0.46	4.83	0.14	0.13	1.57	0.59	1.09	1.16	1.14	0.23	
Sum	100.03	98.52	99.49	99.27	100.25	98.52	99.21	98.97	99.86	99.13	99.02	98.79	100.2	99.93	100.45	99.94	
Rb (ppm)	17	24	12	21	32	47	35	33	35	46	32	22	17	14	35	44	
Sr	492	578	377	729	688	817	731	1103	830	710	880	746	746	848	780	981	
Ba	405	308	145	347	518	410	531	770	511	569	478	381	484	467	463	538	
Cs	0.11	0.18	0.13			0.41		0.7			0.37	0.32					
V	250	299	218	290	306	304	326	222	295	288	256	222	256	269	255	245	
Cu	80	238	42	80	73	41	109	10	76	130	63	56	57	150	79	48	
Cr	954	762	334	451	767	467	258	366	542	349	457	563	530	514	10	407	
Co	122	95	81	72	54	78	84	36	67	71	104	104	65	81	111	63	
Ni	606	298	184	296	487	197	144	14	207	157	336	503	310	303	295	327	
Sc	32	44.1	26.7			36		25			26	25.2					
Y	25.63					30.75	30.76	43.55			32.8	30.58					
Zr	220	278	211			354		275			268	276					
Hf	4.6	5.7	4.16			7.1		5.9			5.4	5.97					
Ta	3.9	4.2	1.68			5.2		6.7			4.1	3.6					
Nb	54.6	58.8	23.52			72.8		93.8			57.4	50.4					
La	48.52	38.8	17.2			62.96	63.1	99.72			70.98	52.08					
Ce	87.93	76	34.2			122.29	113.44	178			122.7	95.56					
Nd	40.77					59.79	50.73	78			58.61	49.57					
Sm	8.46	7.03	4.71			12.13	9.91	14.7			12.15	10.87					
Eu	2.42	3.01	2.21			3.39	2.81	4.19			3.52	3.34					
Tb	0.76	0.86	0.83			1.09		1.19			1.06	1.12					
Gd	6.99					9.4	7.92	11.11			9.62	9.39					
Dy	5					6.39	5.99	8			6.52	6.31					
Er	2.28					2.59	2.53	3.56			2.68	2.43					
Yb	1.81	2.13	2.09			1.89	2.18	3.05			1.95	1.66					
Lu	0.27					0.28	0.32	0.46			0.28	0.24					
Th	4.4	3.84	1.87			5.49		10.5			4.69	4.19					
U	1.09	1.01	0.45			1.49		2.18			1.39	0.97					

Rock type	Basalt																
Sample	2A	2B	B	2D	D	A	T	U	B18	B22	B11	B13	B4	B10	B6	B19	B49
SiO_2 (wt.%)	42.14	42.17	42.95	44.34	45.25	41.6	44.11	44.24	42.69	42.94	45.82	44.84	44.52	50.78	46.13	46.53	46.5
TiO_2	3.06	3.14	3.35	3.22	2.88	4.07	3.02	3.35	3.68	0.51	2.86	3.46	3.44	2.41	3.55	3.16	3.53
Al_2O_3	11.92	11.85	10.82	11.86	13.28	11.52	12.11	13.34	12.39	13.37	12.88	12.73	13.08	13.09	14.45	13.09	15.9
Fe_2O_3*	14.21	14.29	13.13	13.17	13.14	14.48	13.89	13.24	14.57	13.94	13.03	14.08	13.54	11.77	12.99	13.44	13.8
MnO	0.18	0.18	0.2	0.17	0.17	0.2	0.17	0.18	0.19	0.19	0.17	0.18	0.19	0.15	0.17	0.17	0.18
MgO	11.33	11.35	12.63	12.07	9.89	10.96	11.97	10.55	10.21	8.64	9.43	10.12	10.32	7.91	6.47	8.87	4.55
CaO	11.13	11.05	10.29	10.02	10.14	9.91	8.44	9.75	11.43	12.06	10.58	10.15	9.79	8.41	10.27	10.5	10.1
Na_2O	3.43	3.56	3.08	2.89	2.64	3.18	2.41	3.16	3.13	2.98	3.1	3.19	3.14	2.74	3.32	2.94	3.4
K_2O	1.54	1.18	1.36	0.92	0.71	1.35	1.16	1.62	1.31	1.62	0.91	1.48	1.48	0.85	1.85	0.63	1.89
P_2O_5	1.17	1.16	0.82	0.83	0.87	0.9	0.73	0.75	0.68	0.51	0.79	0.58	0.79	0.23	0.63	0.47	0.73
LOI	0.03	0.11	0.36	0.04	1.25	0.66	1.65	0.29	0.04	0.46	0.16	0.32	0.04	0.36	0.08	0.05	0.04
Sum	100.14	100	98.99	99.53	100.2	98.83	99.66	100.5	100.32	96.3	99.41	100.49	100.33	98.7	99.91	99.75	100
Rb (ppm)	16	22	41	34	22	46	10	23	34	38	17	31	30	14	33	14	47
Sr	1025	1030	926	789	784	1012	580	849	839	753	773	720	822	303	707	540	905
Ba	571	573	575	409	406	588	335	463	456	524	388	443	454	180	498	262	589
Cs	0.37		0.38				0.1	0.49									
V	229	239	293	237	228	319	228	252	294	332	224	260	258	212	292	282	243
Cu	39	44	48	60	120	40	46	43	86	143	66	56	56	37	50	72	113
Cr	475	450	481	514	359	341	897	10	416	274	357	397	387	420	230	429	61
Co	43	55	12	74	125	52	110	80	84	74	75	75	63	117	55	83	56
Ni	329	329	399	407	316	274	460	322	239	134	288	268	307	260	120	247	68
Sc	24.3		23				25	28									
Y	34.23		34.16				34.1	38.25									
Zr	319		330				268	371									
Hf	6.31		6.3				5.3	7.5									
Ta	5.01		4.8				3.1	4.99									
Nb	70.14		67.2				43.4	69.86									
La	85.6		79.93				41.36	55.17									

(*continued on next page*)

Table 6 (*continued*)

Rock type	Basalt															
Sample	2A	2B	B	2D	D	A	T	U	B18	B22	B11	B13	B4	B10	B6	B19	B49
Ce	152.44		126.14				72.83	107.8									
Nd	70.63		54.42				42.77	53.08									
Sm	14.14		12.47				10.03	11.84									
Eu	4.04		3.72				3.15	3.56									
Tb	1.24		1.05				1.14	1.26									
Gd	10.7		10.61				8.8	9.64									
Dy	7.05		6.51				6.49	7.2									
Er	2.6		2.71				2.43	3.12									
Yb	1.78		1.89				1.81	2.44									
Lu	0.24		0.37				0.27	0.34									
Th	6.33		5.66				3.32	5.64									
U	1.58		1.49				0.8	1.61									

Rock type	Basalt										
Sample	B31	B50	B45	B15	B9	X	V	W	B61	B62	Q
SiO_2 (wt.%)	42.01	44.28	41.05	41.83	45.98	45.11	45.17	45.48	45.27	48.28	46.46
TiO_2	3.12	3.39	3.23	3.38	3.05	3.53	3.59	3.53	3.42	2.78	2.94
Al_2O_3	11.73	12.95	12.16	12.26	12.14	13.66	14.23	13.65	10.79	13.64	14.68
Fe_2O_3*	14.07	13.73	14.76	13.91	13.13	12.91	13.44	12.74	12.94	11.85	12.47
MnO	0.19	0.2	0.19	0.18	0.17	0.16	0.18	0.18	0.19	0.17	0.21
MgO	11.43	7.12	11.12	11.01	10.43	8.6	6.6	7.82	10.14	7.3	6.02
CaO	11.13	12.49	11.32	10.77	10.44	9.29	11.26	10.82	12.26	10.4	10.77
Na_2O	3.33	2.57	3.9	3.57	2.76	2.78	3.06	2.98	2.39	3.25	2.73
K_2O	1.36	1.57	1.49	1.43	0.98	0.96	1.38	1.62	1.24	1.38	2.02
P_2O_5	1.07	0.56	1.21	0.96	0.63	0.78	0.72	0.81	0.75	0.66	0.45
LOI	0.34	0.48	0.18	0.3	0.39	1.02	0.06	0.55	0.48	0.33	0.05
Sum	99.1	99.34	100.25	99	99.32	98.8	99.69	100.18	99.87	100.12	98.8
Rb (ppm)	32	34	36	34	18	18	23	25	43	35	44
Sr	1058	829	1091	905	616	764	794	879	698	665	765
Ba	580	493	600	494	353	466	474	526	474	462	611
Cs	0.26		0.36	0.31	0.11			0.33		0.43	0.45
V	242	331	241	259	236	241	302	272	313	256	305
Cu	55	149	43	55	53	62	111	73	118	35	128
Cr	497	267	421	444	472	295	195	334	777	346	499
Co	64	67	68	89	64	81	70	55	111	68	73
Ni	306	137	283	296	300	232	146	169	254	125	107
Sc	25.2		24.8	25.9	26.1			27.8		21.3	27
Y								39.42			31.1
Zr	311		389	317	203			399		420	324
Hf	6.03		7.02	6.6	5.52			8.16		8.8	6.5
Ta	5.43		5.64	4.91	3.66			5.25		6.3	4.7
Nb	76.02		78.96	68.74	51.24			73.5		88.2	65.8
La	69.5		53.8	53.8	31.8			62.9		57.8	55.27
Ce	141		131	98.2	67.1			120.85		121	109.46
Nd								62.11			53.67
Sm	10.3		10.9	9.17	7.08			13.53		10.2	10.58
Eu	4.31		4.72	3.93	3			3.98		4.25	3.02
Tb	1.18		1.34	1.22	0.96			1.36		1.27	1
Gd								10.94			8.19
Dy								7.7			5.95
Er								3.1			2.64
Yb	2.16		2.24	2.01	1.95			2.37		2.82	2.15
Lu								0.34			0.33
Th	5.86		6.86	4.93	3.05			5.8		8.44	5.59
U	1.59		2.01	1.37	1.49			1.6		2.24	1.48

Rock type	Hawaiite								Mugearite	
Sample	B47	B21	F	S	K	Y	B56	B63	B25	G
SiO_2 (wt.%)	47.22	43.74	46.21	44.94	45.39	48.36	46.87	50.59	53.46	54.07
TiO_2	3.19	3.29	3.57	3.18	3.12	2.99	3.03	3.05	2.43	2.38
Al_2O_3	14.91	16.01	16.47	16.31	16.6	17.73	15.21	15.52	16.24	16.29
Fe_2O_3*	12.93	14.03	11.03	13.8	10.17	10.33	11.11	11.18	10.64	10.43
MnO	0.18	0.24	0.18	0.24	0.19	0.15	0.18	0.16	0.15	0.14
MgO	5.38	4.59	4.95	4.27	3.66	3.82	5.53	3.91	2.73	2.82
CaO	9.68	9.15	9.73	9.5	8.38	8.86	8.74	8.01	6.99	7.01
Na_2O	3.31	4.02	3.57	4.27	5.09	4.1	4.85	3.78	3.57	3.41
K_2O	1.88	2.26	2.22	2.08	3.08	2.2	2.54	2.15	2.22	2.24
P_2O_5	0.7	0.91	0.83	1.11	0.96	0.87	0.71	0.9	0.59	0.56
LOI	0.8	0.7	1.31	0.37	2.18	0.53	1.21	0.91	0.52	1.04
Sum	100.18	98.94	100.07	100.07	98.82	99.94	99.98	100.16	99.54	100.39
Rb (ppm)	44	67	49	48	69	48	67	57	59	49
Sr	702	1156	1077	1181	1662	1029	1201	892	742	753

Table 6 (*continued*)

Rock type	Hawaiite								Mugearite	
Sample	B47	B21	F	S	K	Y	B56	B63	B25	G
Ba	523	806	720	792	963	630	674	655	647	632
Cs	0.32	0.6	0.65	0.86	0.35	0.54	0.62	0.22		0.96
V	284	237	267	225	208	200	204	249	234	242
Cu	44	10	34	10	19	48	37	10	10	10
Cr	163	25	10	387	17	51	155	34	26	29
Co	80	60	110	23	10	26	47	46	45	41
Ni	79	31	78	18	12	58	102	21	29	22
Sc	29.1	18.5	20	19	37	17.2	19.5	28.7		18
Y			42.58	44.04	48.8	41.5				35.28
Zr	389	389	470	414	197	452	694	282		442
Hf	7.88	8.36	8.7	8.8	5.5	9.16	11.8	6.2		8.3
Ta	5.63	9.6	6.9	8.5	5.1	6.89	11.5	4.4		4.9
Nb	78.82	134.4	96.6	119	71.4	96.46	161	61.6		68.6
La	79.7	91.5	93.9	111.78	135.77	81.02	102.9	52.7		68.91
Ce	103	165	153.39	192.67	250.89	151.34	209	87.8		132.12
Nd			73.55	82.47	111.06	69.3				61.81
Sm	8.54	11.1	15.05	15.44	20.66	14.19	12.1	7.24		12.13
Eu	3.48	4.54	4.32	4.31	5.67	4.14	4.8	3.29		3.19
Tb	1.05	1.25	1.42	1.39	0.91	1.42	1.3	1.04		1.08
Gd			11.68	11.64	14.5	11.08				8.97
Dy			8.2	8.17	9.49	7.97				6.49
Er			3.44	3.71	3.7	3.27				2.95
Yb	2.69	3.74	2.65	3.04	2.67	2.46	0.14	2.48		2.61
Lu			0.37	0.46	0.37	0.35				0.37
Th	7.44	10.22	7.09	9.82	5.6	8.57	13.4	6.26		9.33
U	1.89	2.28	2.07	2.57	1.43	1.98	3.71	1.61		2.23

LOI = loss on ignition.

Rb contents remain low in all rocks (<70 ppm). Sr contents are high in basalts (1030–330 ppm) reflecting the cumulative character of plagioclase. In contrast, the Ba contents, low in basalts (145–770 ppm), increase slightly in hawaiites (523–963 ppm).

Th/Ba, Th/Rb and Th/U ratios in alkali basalts are almost constant at 0.009–0.010, 0.11–0.39 and 3.50–4.15, respectively. These ratios are rather similar and coincide with values reported for Pagalu in the oceanic section of the Cameroon Line (Lee et al., 1994), with typical HIMU oceanic island basalts (e.g., Tubuaii in the Pacific Ocean, Chauvel et al., 1992) and with average values reported for HIMU basalts (Th/Ba = 0.013–0.020, Th/Rb = 0.20–0.29, Th/U = 2.65–3.61; Sun and McDonough, 1989). LILE/HFSE ratios (e.g. Ba/Nb: 5.63–9.28) and LREE/HFSE ratios (e.g. La/Nb: 0.73–1.23) are high in alkali basalts. LILE/LREE ratios (e.g. Ba/La: 6.73–11.05) are high but HFSE/HFSE ratios (e.g. Zr/Nb: 2.93–8.97) are low in the alkali basalt.

Normalized-primitive mantle (McDonough and Sun, 1995) trace element patterns are shown in Fig. 7. Patterns are strongly fractionated ($(La/Yb)_N$ = 5.0–29.0) and characterized by negative K anomalies and slight negative Hf anomalies. All basalt patterns of the Bioko Island volcanic rocks are similar to those of typical OIB patterns of HIMU component (Sun and McDonough, 1989) with positive Nb and Ta anomalies and negative K anomalies.

All the Bioko Island volcanic rocks are rich in LREE with La values between 17.2 and 62.96 and Lu between 0.27 and 0.28 (Table 6). Mantle-normalized REE abundances (McDonough and Sun, 1995) are shown in Fig. 8. The patterns for the basalts are very similar, relatively steep and roughly parallel, showing relative LREE enrichment. Compositional variation within these samples is likely to have been dominantly controlled by addition/subtraction of REE-deficient ferromagnesian phases. The hawaiite samples also have normalized REE patterns closely similar to those of the alkali basalts. The values of the $(Ce/Yb)_n$ ratios of alkali basalts are comprised between 4 and 24 whereas other basalts of the Cameroon Line have values comprises between 12 and 22 (Ngounouno et al., 2001).

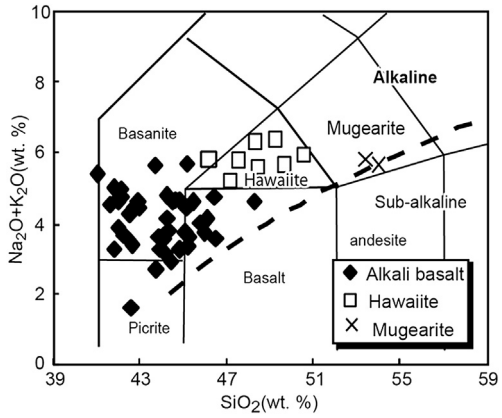

Figure 4. Total alkali–silica diagram according to Le Bas et al. (1986). The subdivision (dashed line) of volcanic rocks into alkaline and sub-alkaline rocks is after Miyashiro (1978).

4.3.2. Sr-Nd-Pb isotopic chemistry

Sr-Nd-Pb isotopic concentrations for five representative samples from Bioko Island are given in Table 7 and plotted in Fig. 9. They display fairly restricted range in Sr-isotopic ratios (0.7034–0.7040, average 2-error: 0.00002). Nd isotopic ratios of Bioko Island volcanic rocks are low and fall in the narrow range of 0.512769 and 0.51286. As shown in a diagram of ε_{Nd} vs. $^{87}Sr/^{86}Sr$ (Fig. 9a), the Bioko Island volcanic rocks plot in the depleted field relative to bulk silicate Earth (BSE). Generally, this trend is similar to trends of other mafic alkaline rocks from the CHL (Halliday et al., 1988, 1990; Lee et al., 1994; Marzoli et al., 2000; Yokoyama et al., 2007; Nkouathio et al., 2008). One sample falls in the field of mantle array. Almost the samples display positive ε_{Nd} (+2.56 to +4.33; same reference as Sr) compositions point to a slightly depleted upper mantle source, Pb isotopic ratios of basaltic rocks are still higher for $^{206}Pb/^{204}Pb$ (20.032–20.368), $^{207}Pb/^{204}Pb$ (15.65–15.69) and $^{208}Pb/^{204}Pb$ (39.80–40.21) compared to those of Cameroon Volcanic Line (Halliday et al., 1990; Yokoyama et al.,

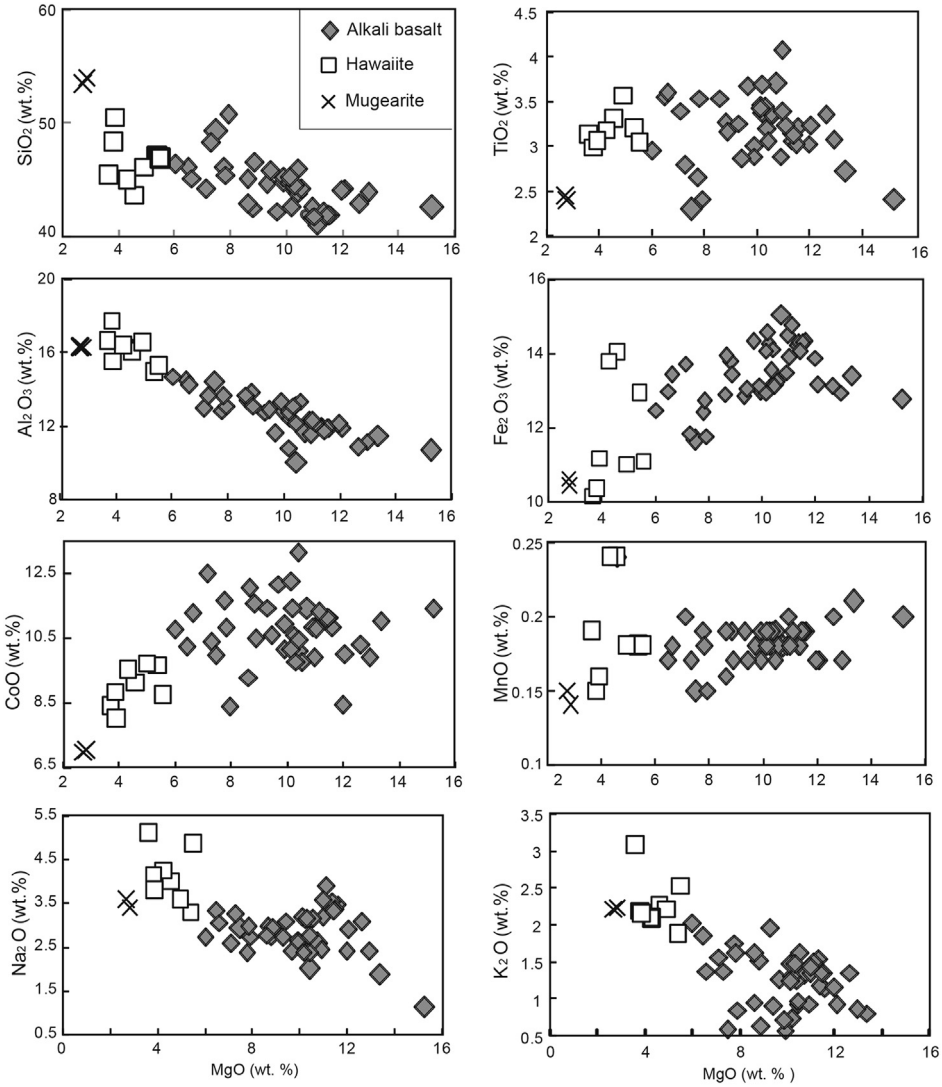

Figure 5. Harker diagrams showing variations of major elements oxides with MgO (wt. %), for Bioko Island volcanic rocks.

2007) and belong to HIMU-type component (Zindler and Hart, 1986). Otherwise, the Pb isotopic characteristics of Bioko Island volcanic rocks fall slightly on the Northern Hemisphere Reference Line (NHRL) of Hart (1984) in the $(^{206}Pb/^{204}Pb)_i$ vs. $(^{207}Pb/^{204}Pb)_i$ plot (Fig. 9b). In the $(^{206}Pb/^{204}Pb)_i$ vs. $(^{87}Sr/^{86}Sr)_i$ (Fig. 9c) plot, the samples plot above or around the LoNd array (Hart, 1984; Hart et al., 1986; Hart, 1988), and show a linear trend between HIMU and EM1 components. However, Sr, Nd and Pb isotopic ratios of Bioko Island volcanic rocks are not typical of HIMU-type of St-Helene (Chaffey et al., 1989) neither those of whole CHL source for which Déruelle et al. (2007) suggest the FOZO-type component when projecting the whole isotopic data of CHL in many diagrams. For the Bioko Island volcanic rocks, the model proposed suggests the contribution of EM1.

5. Discussion

5.1. Petrological implications

The samples have LOI of 0.25–2.53 wt.%, and their Ba/Rb and K_2O/P_2O_5 ratios range from 12.83 to 35.68 and from 0.6 to 34.48, respectively. The Rb/Sr ratios generally increase with increasing of K_2O/P_2O_5 (Fig. 10a) ratios and K_2O + Na_2O decreases with increasing of LOI (Fig. 10c). No significant correlations are observed between Rb and Zr (Fig.10b). These geochemical features, together with the consistency of the dataset in Table 6, suggest that the highly incompatible elements (e.g., Rb, Ba and K) for the samples might have been mobile but that the moderately incompatible elements (e.g. Zr, Th, Hf and LREE) were immobile during low-temperature alteration (Frey et al., 1994). The low Ni and Cr contents and $Mg^{\#}$ for hawaiites suggest that they have undergone considerable crystal fractionation.

Elevated SiO_2 contents, high $^{87}Sr/^{86}Sr$ ratios, low ε_{Nd} values and negative Nb and Ta anomalies are commonly used as indicators of crustal contamination of mafic melts (DePaolo, 1981).

All the basalts have low SiO_2, low $^{87}Sr/^{86}Sr$, high ε_{Nd}, high Nb/La ratios and TiO_2 contents. Such geochemical signatures do not support crustal assimilation or AFC processes (DePaolo, 1981).

5.2. Fractionation model

5.2.1. Major-element modelling

Evolution by crystal fractionation has been modelled for the short differentiation series of Bioko. Despite the restricted

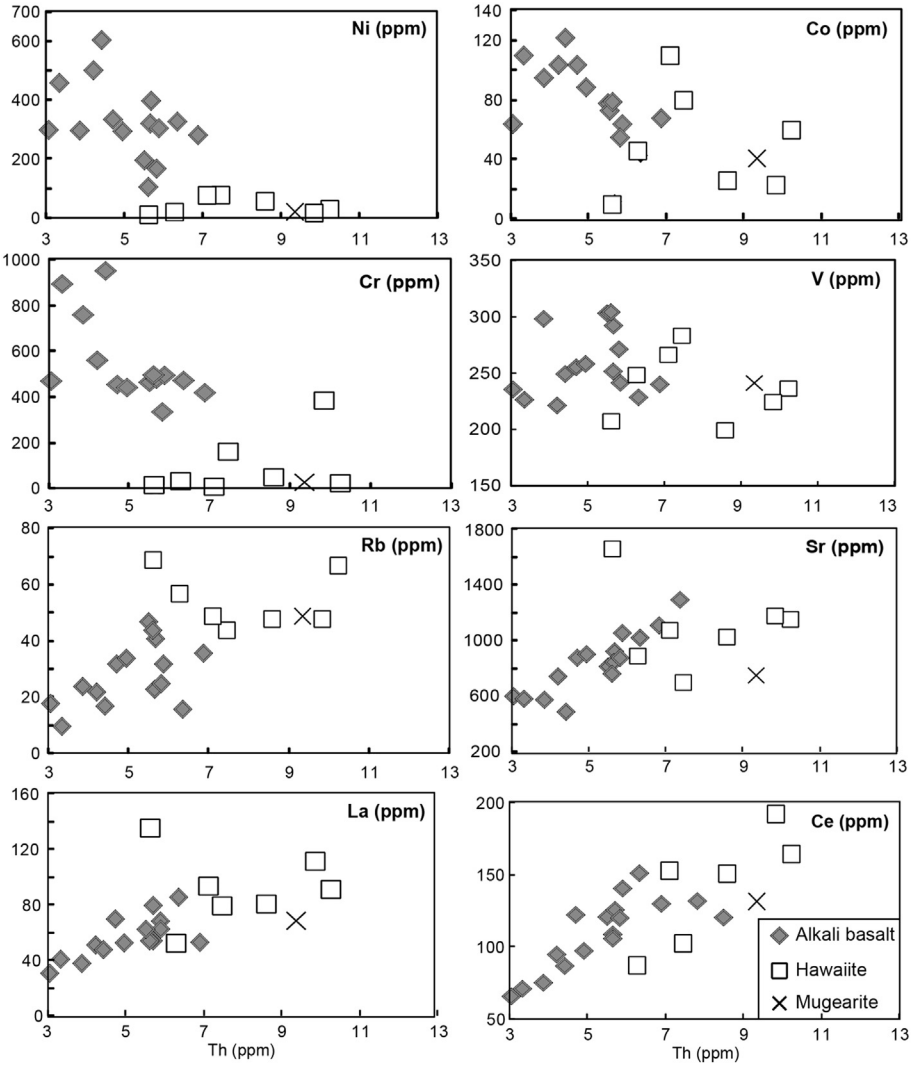

Figure 6. Harker diagrams showing variations of trace elements (ppm) with Th (ppm) for Bioko Island volcanic rocks.

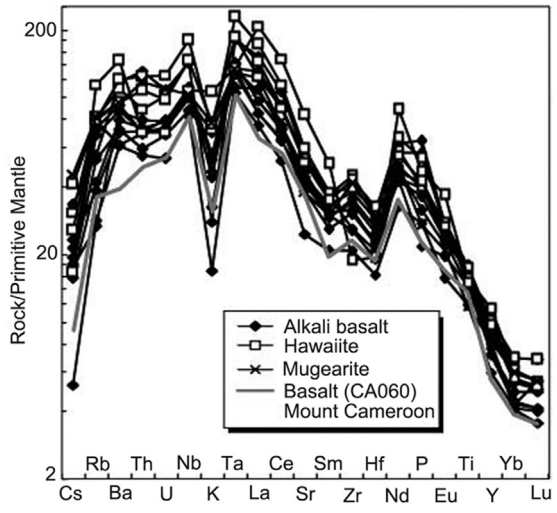

Figure 7. Normalized multi-element (spider) diagrams for representative Bioko Island volcanic rocks, comparing trace element concentrations of alkali basalt from Mount Cameroun (CA060, Yokoyama et al., 2007). Primitive mantle abundances used are from McDonough and Sun (1995).

compositional range observed for the data set, the mineralogical (progressive evolution of mineral compositions with increasing differentiation) and geochemical (regular and progressive major and trace element evolution) data suggest that fractional crystallization played an important role in the differentiation of the rock series.

Fractional crystallization model (DePaolo, 1981) for major element is that of closed-system for which calculations consider the least-square mass-balance calculation with the sum of the squares of the residuals (Σr^2). We use in our calculation the composition of the core of phenocrysts of all mineral phases which are implicated in the differentiation and have been obtained from microprobe analyses in respective parental rock to have a calculated daughter rock. In this model, we choice the composition of (D) as that of parental magma because of its high MgO content (9.89 wt.%) when compared to that of other basaltic rocks and its high content of transitional element (Ni = 316 ppm, Co = 125 ppm and Cr = 359 ppm). The result shows that fractionation of basalt (D) by removal of olivine (6.9 wt.%), plagioclase (0.3 wt.%), clinopyroxene (0.7 wt.%) and oxides (0.1 wt.%) gives a silicate liquid that composition is similar to that of hawaiite (F) with a good Σr^2 (=0.6).

This model precludes an evolution through a closed-system fractional crystallization alone and attests that the rocks

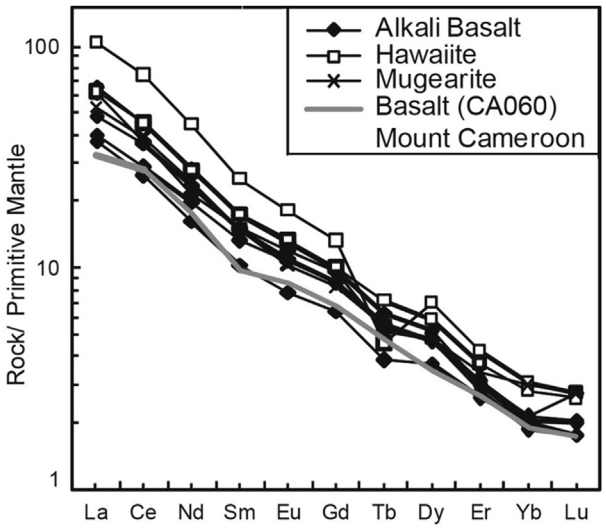

Figure 8. Primitive mantle-normalized REE plots for Bioko Island volcanic rocks. A plot of the alkali basalt from Mount Cameroon (CA060, Yokoyama et al., 2007) is also included for comparison. The primitive mantle abundances used are from McDonough and Sun (1995).

constitute a single series that the differentiation is essentially controlled by fractional crystallization. The magma mixing has for now no effect on the differentiation processes.

5.2.2. Trace-element modelling

A closed-system assimilation and fractional crystallization following Eq. (1) (DePaolo, 1981) which becomes Raleigh's law (Eq. (2), because of the lack of wall rock assimilation, $r = 0$) have been tested to account for the derivation of hawaiite from basalt.

$$\frac{C_1}{C_0} = F^{-z} + \frac{r}{r-1}\frac{C_a}{C_0 z}\left(1 - F^{-z}\right)$$
$$z = \frac{r + D - 1}{r - 1} \quad (1)$$

where r is assimilation/crystallization ratios (<1, in general between 0 and 0.5). This equation becomes Eq. (2) by replacing r by 0 ($r = 0$, as there is not supposed crustal contamination of these rocks):

$$C_1^i = C_0^i F\left(D^i - 1\right) \quad (2)$$

where C_1^i is the concentration of trace element i in the liquid, C_0^i is the concentration of trace element i in the consider parental magma, F is the weight proportion of the fractionated parental liquid and D^i, the bulk distribution coefficient for element i. Values of D^i are estimated by combining the proportion of minerals that has been obtained from the major-element modelling, with mineral/liquid partition coefficient from Halliday et al. (1995).

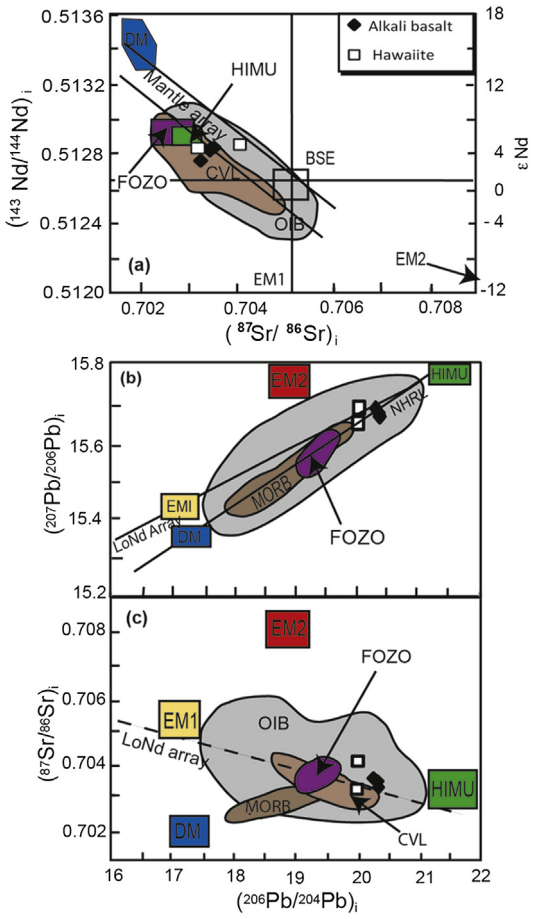

Figure 9. (a) $(^{87}Sr/^{86}Sr)_i$ vs. $(^{143}Nd/^{144}Nd)_i$; (b) $(^{206}Pb/^{204}Pb)_i$ vs. $(^{207}Pb/^{206}Pb)_i$; (c) $(^{206}Pb/^{204}Pb)_i$ vs. $(^{87}Sr/^{86}Sr)_i$ for Bioko Island volcanic rocks. The fields of HIMU, OIB, FOZO, Dupal OIB, EMI and EM2 are from Hamelin and Allègre (1985), Zindler and Hart (1986), Hart (1984, 1988), Hart et al. (1992), Hawkesworth et al. (1984) and Weaver (1991). Low Nd (LoNd) array and Northern Hemisphere Reference Line (NHRL) are from Hart (1984). The fields for Atlantic-Pacific MORB are from Hamelin and Allègre (1985) and the references therein. Literature data for CHL where compiled from Halliday et al. (1988, 1990), Lee et al. (1994), Marzoli et al. (1999, 2000), Yokoyama et al. (2007) and Nkouathio et al. (2008).

Parameters D^i, F and C_0^i are introduced in Eq. (2) to calculate the trace-element concentrations of the daughter liquid. The results are shown in Fig. 11 as the multi-element normalized to the primitive mantle (McDonough and Sun, 1995) patterns where in each case are presented the pattern of the considered parental magma, that of measured data, and that of calculated daughter liquid. Fig. 11 shows that compositions of the daughter liquid are quite similar to that of measured liquid except for Rb. This discrepancy can be explained by the non fractionation of the mineral phases which assimilate Rb or to underestimation of the Rb distribution coefficient used in the model. Resorbtion of olivine indicates a P-T conditions and

Table 7
Nd, Sr and Pb isotopic data from Bioko Island volcanic rocks.

	Sample	$^{87}Sr/^{86}Sr$	Rb (ppm)	Sr (ppm)	2 s	Nd (ppm)	Sm (ppm)	ε_{Nd}	$^{143}Nd/^{144}Nd$	$^{206}Pb/^{204}Pb$	$^{207}Pb/^{204}Pb$	$^{208}Pb/^{204}Pb$
Basalt	N2	0.703441	17	492	0.000011	40.77	8.46	3.71	0.512828	20.353	15.68	40.17
	H	0.703248	32	880	0.000011	58.61	12.15	2.56	0.512769	20.368	15.67	40.21
	B10	0.703518	17.5	303	0.000008			4	0.512843	20.298	15.69	40.05
Hawaiite	B59	0.70406	73	926	0.000012			4.33	0.51286	20.044	15.69	39.8
	K	0.703208	69	162	0.000008	111.06	20.66	3.92	0.512839	20.032	15.65	39.86

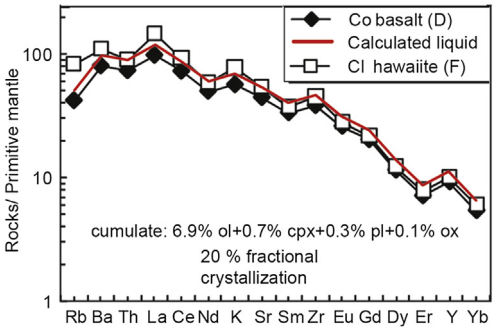

Figure 10. Primitive mantle-normalized (McDonough and Sun, 1995) trace element patterns showing calculated liquid composition produced by 20% of fractional crystallization from the Bioko Island volcanic rocks. Sample (D) represent parent rock. Composition of the hawaiite (F) is indicated for comparison.

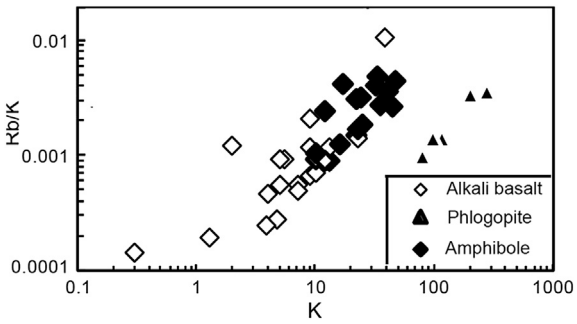

Figure 12. Rb/K vs. K plot for the alkaline rocks from the Bioko Island. Phlogopite (closed lozenges) and amphibole (crosses) compositions are from O'Reilly et al. (1991), Adam et al. (1993) and Ionov and Hofmann (1995).

chemistry disequilibria, which could result as the growth of Ti-augite (low pressure phase with high rate of growth (Kogiso et al., 2003)) from a decompression of the rocks.

5.3. Source characteristics

Some features of the primitive mantle-normalized incompatible element patterns of Bioko Island volcanic rocks are suggestive of trace-element fractionation caused by a residual minor mantle phases. Bioko basalts display marked depletion in K and Rb compared to other incompatible trace elements in (Fig. 7) consisting with the presence of a residual minor K-bearing phase in the source region (as noted by Ngounouno et al., 2005) for monchiquites from Tchircotché in the Benue valley, northern Cameroon. The presence of a small negative Sr anomaly may suggest that this potassic phase was K-amphibole. In the absence of any other phase which fractionates Sr (e.g. apatite, plagioclase), the anomaly in this element may be a characteristic of the source. Negative anomalies of Rb and K in primitive mantle-normalized diagrams and Rb/K vs. K (Fig. 12) covariations suggest that amphibole was the major OH-bearing mineral phase. As an alternative hypothesis, it has been suggested (i.e. Chauvel et al., 1992) that K negative anomaly is a characteristic of the source of the alkali basalts with HIMU Pb isotope signatures, such as the alkali basalts of the Cameroon Line (Halliday et al., 1990). Such relative K depletion could be related to the alteration and/or the deshydratation of the oceanic crust during a subduction or mantle metasomatism.

The steep REE patterns are typical of that of the alkaline rocks with a probable presence of the garnet in the residue of the partial melting. The strong depletion of heavy REE in alkali basalts could reflect either the occurrence of garnet as a residual phase during partial melting in the mantle. Melting should have taken place below the lithosphere, at great depth (>80 km) in the garnet stability field. The $(La/Ce)_N$ ratios (1.4–1.6) are roughly similar for all the rocks from the three Bioko volcanoes but are significantly higher than those from the neighbouring continental volcanoes of Mount Etinde (1.25–1.27; Nkoumbou et al., 1995) and Mount Cameroon (1.16–1.30; Chauvel et al., 2005 and unpublished data) and from oceanic volcanoes of Principe (0.90–1.33; Fitton and Hughes, 1977) and Sao Tomé (1.24–1.31; data after Halliday et al., 1990) which suggests the existence of a distinct magma source under Bioko island.

5.4. Plume-lithosphere interaction

Fig. 13 uses the Ce/Y and Zr/Nb ratios of the Bioko rocks to model the degree of partial melting from a fertile garnet lherzolite containing 1% of amphibole for the Bioko volcanics rocks. The majority of the Bioko Island volcanics rocks require <3% melting of a mantle source with modal garnet variations of 0–4%. Thus, the high La/Sm (3.65–6.78) and Sm/Yb (2.25–7.94) ratios, similar to those of Reunion (Lassiter and DePaolo, 1997) indicate derivation by low degrees of melting of a garnet-bearing mantle source. This interpretation is supported by the high LREE, TiO_2, and P_2O_5 contents, the high La/Yb ratios and the relatively low HREE concentrations of these samples. Compositional ranges most likely reflect derivation from a heterogeneous mantle source. Nb/U and Th/La ratios for most samples fall near or within the ranges for OIB (Weaver, 1991), similar to those of some basalts of the Cameroon Line (Nkouatkio et al., 2002; Yokoyama et al., 2007). Nb/Th ratios are close to that estimated for OIB (Sun and McDonough, 1989). The OIB like geochemical signatures are also indicated by the high LILE/LREE and LREE/HFSE ratios described above. As shown in Fig. 9, the Pb isotopic compositions for these samples tend to cluster near/toward the estimated HIMU-type OIB source (Hart, 1984; Hart et al., 1986; Hart, 1988; Weaver, 1991). The extremely high Pb isotopic compositions are close to the HIMU-type reservoir characterized by a high $^{206}Pb/^{204}Pb$ ratio of 20.5 (Hart, 1988). These characteristics, together with the enrichment in alkali and highly incompatible

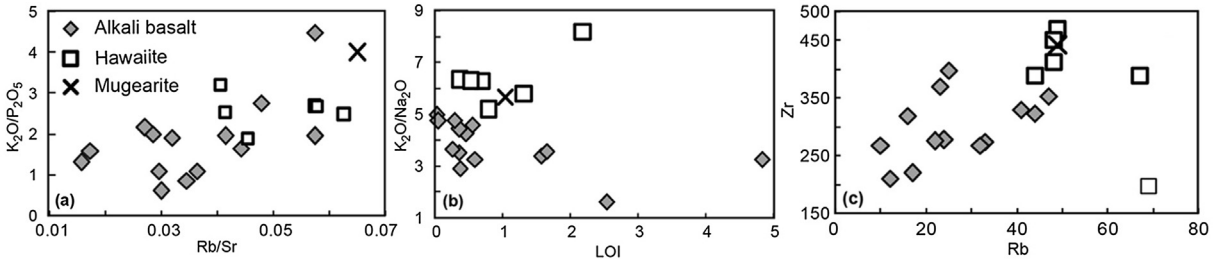

Figure 11. Plots of (a) Rb/Sr vs. K_2O/P_2O_5, (b) LOI (loss on ignition) vs. K_2O/Na_2O and (c) Rb vs. Zr for the Bioko Island volcanic rocks.

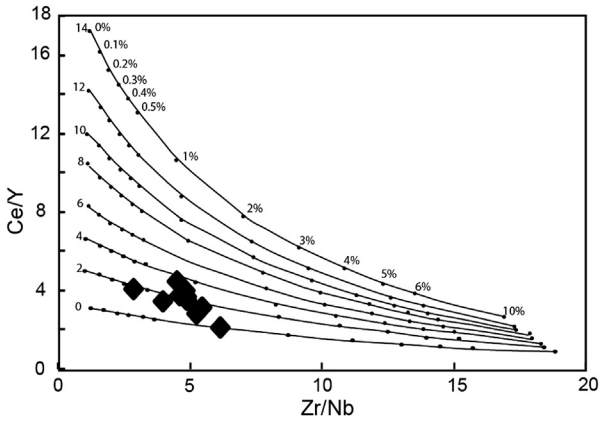

Figure 13. Ce/Y vs. Zr/Nb. This plot indicates partial melting and mineralogical compositions of original mantle under Bioko Island. Same symbols as in Fig. 2. Curved lines denote calculated fractional melts from a fertile peridotite with ca. 2* chondritic abundances of the elements. D-values are from Halliday et al. (1995) and for amphibole, D-values from GERM (http://earthref.org/GERM/), Chazot et al. (1996), Latourrette et al. (1995), Matsui et al. (1977) and Villemant et al. (1981). Tick marks denote melt fraction and numbers at the start of each curve indicate the modal abundance of garnet in the source. The samples with MgO < 7 wt.% are not presented.

trace elements and moderate depletion in Nd isotopic ratios, suggest a potential HIMU-type component in the magma source. However, as illustrated in Fig. 9c, the Bioko Island samples define a linear array that can be attributed to binary mixing. The trends on Sr–Nd–Pb isotopic diagrams also strongly support an origin of binary mixing between an end-member to a HIMU-type source and another end-member component. Pb isotopic compositions plot above the NHRL, and are similar to the southern Hemispheres component (Dupré and Allègre, 1983; Hart, 1984; Hart et al., 1986; Hart, 1988). Such elemental and isotopic signatures could be due to the involvement of a subcontinental lithospheric component in the magma source, assuming that crustal assimilation en route was insignificant.

There are two main types of subcontinental mantle (EM) sources: EM1 (related to carbonatitic metasomatism) and EM2 (attributed to subduction-related metasomatism). An EM1-type source is generally characterized by negative Zr–Hf anomalies and lower $(Hf/Sm)_N$ ratios relative to $(Ta/La)_N$ ratios, whereas an EM2-type source is characterized by negative Nb–Ta anomalies and lower $(Ta/La)_N$ ratios than $(Hf/Sm)_N$ ratios (Hart, 1984; Palacz and Saunders, 1986; Hart, 1988; Weaver, 1991; Carlson, 1995; LaFlèche et al., 1998). The Bioko Island basalts have $(Hf/Sm)_N$ ratios of 0.57–1.16 and $(Ta/La)_N$ ratios of 1.0–1.8, suggesting the involvement of a carbonatitic metasomatised component. On the plots of Sr–Pb and Pb–Pb isotopes (Fig. 9), they have $(^{87}Sr/^{86}Sr)_i$, $(^{207}Pb/^{204}Pb)_i$ and $(^{208}Pb/^{204}Pb)_i$ ratios lower than an EM2-type source with comparable $(^{206}Pb/^{204}Pb)_i$ ratios, and appear to be more compatible with an EM1-type source. It should be noted, however, that the basalts from the Bioko Island have high Ti/Eu ratios (4500–6500) that argue against the direct participation of carbonatitic melts. Thus, we argue that the elemental ratios and Sr, Nd and Pb isotopic compositions for these samples define a binary mixing array between EM1 and HIMU components, supporting our suggestion that they are the products of the plume-lithosphere interaction.

6. Conclusions

Petrographical, mineralogical and geochemical studies on the Bioko Island volcanic rocks reveal them to be alkaline series with co-genetic origin. Petrogenetic processes constrained by calculated models of the series began with the low degree of partial melting (<3%) of HIMU type component source with the residual amphibole in the garnet stability field at the depth of nearly 80 km. Variations of major and trace element content can be related to fractional crystallization implying olivine, clinopyroxene, plagioclase and oxides. The basalts of Bioko Island are geochemically comparable with others basalts of CHL. The elemental and isotopic variability of the Bioko most primary rocks is likely due to low degrees of melting of a heterogeneous garnet-bearing mantle. Furthermore, the magma source reservoir may have contained both HIMU- and EM1-components.

Acknowledgements

The Professor Albert Jambon is acknowledged for providing a grant to Y.F for a one-month stay in France in the “Laboratoire de Magmatologie et de Géochimie Inorganique et Expérimentale” (MAGIE), “Université Pierre-et-Marie-Curie”, Paris 6. The isotopic measurements at the Université Libre de Bruxelles were financially supported by the Ministère des Affaires Economiques (Project SGB/NAT 91-98). The constructive comments of Dr. Yener Eyuboglu are greatly appreciated.

Appendix A. Supplementary data

Supplementary data related to this article can be found at http://dx.doi.org/10.1016/j.gsf.2015.06.003

References

Adam, J., Green, T.H., Sie, S.H., 1993. Proton microprobe determined partitioning of Rb Sr, Ba, Y, Zr, Nb, and Ta between experimentally produced amphiboles and silicate melts with variable F contents. Chemical Geology 109, 29–49.

Aka, F.T., Nagao, K., Kusakabe, M., Sumino, H., Tanyileke, G., Ateba, B., Hell, J., 2004. Symmetrical helium isotope distribution on the Cameroon volcanic line, West Africa. Chemical Geology 203, 205–223.

Ashwal, L.D., Demaiffe, D., Torsvik, T.H., 2002. Petrogenesis of Neoproterozoic granitoids and related rocks from the Seychelles: the case for an Andean-type arc origin. Journal of Petrology 43, 45–83.

Berger, J., Ennih, N., Liégeois, J.P., Nkono, C., Mercier, J.C.C., Demaiffe, D., 2008. A complex multi-chamber magmatic system beneath a late Cenozoic volcanic field: evidence from CSDs and thermobarometry of clinopyroxene from a single nephelinite flow (Djbel Saghro, Morocco). Geological Society of London, Special Publication 297, 509–524.

Carlson, R.W., 1995. Isotopic inferences on the chemical structure of the mantle. Journal of Geodynamics 20, 365–386.

Carignan, J., Hild, P., Mevelle, G., Morel, J., Yeghicheyan, D., 2001. Routine analyses of trace elements in geological samples using flow injection and low pressure on line liquid chromatography coupled to ICP-MS: a study of geochemical reference materials BR, DR-N, UB-N, AN-G and GH. Geostandards Newsletters 25, 187–198.

Chaffey, D.J., Cliff, R.A., Wilson, B.M., 1989. Characterization of the St Helena magma source. In: Saunders, A.D., Norry, M.J. (Eds.), Magmatism in the Ocean Basins, Geological Society of London, Special Publication, 42, pp. 257–276.

Chauvel, C., Hofmann, A.W., Vidal, P., 1992. HIMU–EM: the French Polynesian connection. Earth and Planetary Science Letters 110, 99–119.

Chauvel, C., Dia, A.N., Bulourde, M., Chabaux, F., Durand, S., Ildefonse, P., Gérard, M., Déruelle, B., Ngounouno, I., 2005. Do decades of tropical rainfall affect the chemical compositions of basaltic lava flows in Mt Cameroon? Journal of Volcanology and Geothermal Research 141, 195–223.

Chazot, G., Menzies, M.A., Harte, B., 1996. Determination of partition coefficients between apatite, clinopyroxene, amphibole, and melt in natural spinel lherzolites from Yemen: implications for wet melting of the lithospheric mantle. Geochimica et Cosmochimica Acta 60, 423–437.

Dautria, J.M., Liotard, J.M., Cabanes, N., Girod, M., Briqueu, L., 1987. Amphibole rich in xenoliths and host alkali basalt: petrogenetic constraints and implications on the recent evolution of the upper mantle beneath Ahaggar (Central Sahara, Southern Algeria). Contributions to Mineralogy and Petrology 95, 133–144.

Déruelle, B., N'ni, J., Kambou, R., 1987. Mount Cameroon: an active volcano of the Cameroon line. Journal of African Earth Science 6, 197–214.

Déruelle, B., Moreau, C., Nkoumbou, C., Kambou, R., Lissom, J., Njonfang, E., Ghogomu, R.T., Nono, A., 1991. The Cameroon line: a review. In: Kampunzu, A.B., Lubala, R.T. (Eds.), Magmatism in Extensional Structural Settings. The Phanerozoic African Plate. Springer, Berlin, Germany, pp. 274–327.

Déruelle, B., Ngounouno, I., Demaiffe, D., 2007. The "Cameroon Hot Line" (CHL): a unique example of active alkaline intraplate structure in both oceanic and continental lithospheres. Comptes Rendus Géosciences 339, 589–600.
DePaolo, D.J., 1981. Trace element and isotopic effects of combined wall rock assimilation and fractional crystallization. Earth and Planetary Science Letters 53, 189–202.
Duprè, B., Allègre, C.J., 1983. Pb–Sr isotopic variation in Indian Ocean basalts and mixing phenomena. Nature 303, 142–146.
Enciclopedia Universal Ilustrada 1924. Fernando Poo, Espasa-Calpe SA Hijos de J. Espasa, Madrid 23, 833pp.
Fail, J.P., Montadert, L., Delteil, J.R., Valéry, P., Patriat, P., Schlich, R., 1970. Prolongation des zones de fractures de l'océan Atlantique dans le golfe de Guinée. Earth and Planetary Science Letters 7, 413–419.
Fitton, J.G., Hughes, D.J., 1977. Petrochemistry of volcanic rocks of the island of Principe, Gulf of Guinea. Contributions to Mineralogy and Petrology 64, 247–272.
Fitton, J.G., 1987. The Cameroon line, West Africa: a comparison between oceanic and continental alkaline volcanism. In: Fitton, J.G., Upton, B.G. (Eds.), Alkaline Igneous Geological Society of London, special Publication, 30, pp. 273–291.
Frey, F.A., Garcia, M.O., Roden, M.F., 1994. Geochemical characteristics of Koola volcano: implications of intershield geochemical differences among Hawaiian volcanoes. Geochimica et Cosmochimica Acta 58, 1441–1462.
Halliday, A.N., Dickin, A.P., Fallick, A.E., Fitton, J.G., 1988. Mantle dynamics: a Nd, Sr, Pb and O isotopic study of the Cameroon line volcanic chain. Journal of Petrology 29, 181–211.
Halliday, A.N., Davidson, J.P., Holden, P., DeWolf, C., Lee, D.C., Fitton, J.G., 1990. Trace fractionation in plumes and the origin of HIMU mantle beneath the Cameroon line. Nature 347, 523–528.
Halliday, A.N., Lee, D.C., Tommasini, S., Davies, G.R., Paslick, C.R., Godfrey, Fitton, J.G., James, D.E., 1995. Incompatible trace elements in OIB and MORB and source enrichment in the sub-oceanic mantle. Earth and Planetary Science Letters 133, 379–395.
Hamelin, B., Allègre, C.J., 1985. Large scale regional units in the depleted upper mantle revealed by an isotopic study of the south–west India ridge. Nature 315, 196–198.
Hart, S.R., 1984. The Dupal anomaly: a large-scale isotopic anomaly, in the southern hemisphere. Nature 309, 753–756.
Hart, S.R., Gerlach, D.C., White, W.M., 1986. A possible new Sr–Nd– Pb mantle array and consequences for mantle mixing. Geochimica et Cosmochimica Acta 50, 1551–1557.
Hart, S.R., 1988. Heterogeneous mantle domains: signature, genesis and mixing chronologies. Earth and Planetary Science Letters 90, 273–296.
Hart, S.R., Hauri, E.H., Oschmann, L.A., Whitehead, J.A., 1992. Mantle plumes and entrainment: isotopic evidence. Science 256, 517–520.
Hawkesworth, C.J., Rogers, N.W., van Calsteren, P.W.C., Menzies, M.A., 1984. Mantle enrichment processes. Nature 311, 331–335.
Hedberg, J.D., 1969. A Geological Analysis of the Cameroon Trend. Ph. D. Thesis. University of Princeton, N.J., U.S.A., p. 188.
Ionov, D.A., Hofmann, A.W., 1995. Nb-Ta-rich mantle amphiboles and micas: implications for subduction-related metasomatic trace element fractionation. Earth and Planetary Science Letters 131, 341–356.
Kogiso, T., Hirschmann, M.M., Frost, D.J., 2003. High-pressure partial melting of garnet pyroxenite: possible mafic lithologies in the source of ocean island basalts. Earth and planetary Science Letters 216, 603–617.
LaFlèche, M.R., Camiré, G., Jenner, G.A., 1998. Geochemistry of post-Acadian, Carboniferous continental intraplate basalts from the Maritimes basin, Magdalen islands, Québec, Canada. Chemical Geology 148, 115–136.
Lassiter, J.C., DePaolo, D.J., 1997. Plume/lithosphere interaction in the generation of continental and oceanic flood basalts: chemical and isotopic constraints. In: Mahoney, J.J., Coffin, M.F. (Eds.), Large Igneous Province: Continental, Oceanic, and Planetary Flood Volcanism, American Geophysical Union Geophysical Monograph 100, pp. 335–355.
Latourrette, T., Hervig, R.L., Holloway, J.R., 1995. Trace-element partitioning between amphibole, phlogopite, and basanite melt. Earth and Planetary Science Letters 135, 13–30.
Lee, D.C., Halliday, A.N., Fitton, J.G., Poli, G., 1994. Isotopic variations with distance and time in the volcanic islands of the Cameroon Line: evidence for a mantle plume origin. Earth and Planetary Science Letters 123, 119–138.
Le Bas, M.J., Le Maitre, R.W., Streckeisen, A., Zaneltin, B., 1986. A chemical of volcanic rocks based on the total alkali silica diagram. Journal of Petrology 27, 745–750.
Leeman, W.P., 1978. Distribution of Mg between olivine and silicate melt and its complications regarding melt structure. Geochimica et Cosmochimica Acta 42, 789–800.
Leake, B.E., 20 co-authors, 1997. Nomenclature of amphiboles: report of the subcommitee on amphiboles of the International Mineralogical Association commission on new minerals and mineral names. Mineralogical Magazine 61, 295–321.
Marsh, B.D., 1988. Crystal size distribution (CSD) in rocks and the kinetics and dynamics of crystallization. 1. Theory. Contributions to Mineralogy and Petrology 99, 277–291.
Marzoli, A., Renne, P.R., Peccirillo, E.M., Castorina, F., Bellieni, G., Melfi, A.G., Nyobe, J.B., N'ni, J., 1999. Silicic magmas from the continental Cameroon volcanic line (Oku, Bambouto and Ngaoundere): $^{40}Ar–^{39}Ar$ dates, petrology, Sr–Nd–O isotopes and their petrogenetic significance. Contributions to Mineralogy and Petrology 135, 133–150.
Marzoli, A., Peccirillo, E.M., Renne, P.R., Bellieni, G., Iacumin, M., Nyobe, J.B., Tongwa, A.T., 2000. The Cameroon volcanic line revisited: petrogenesis of continental basaltic magmas from lithospheric and asthenospheric mantle sources. Journal of Petrology 41, 87–109.
Matsui, Y., Onuma, N., Nagasawa, H., Higuchi, H., Banno, S., 1977. Crystal structure control in trace element partition between crystal and magma. Tectonics 100, 315–324.
Mbowou, G.I.B., Lagmet, C., Nomade, S., Ngounouno, I., Déruelle, B., Ohnenstetter, D., 2012. Petrology of the late Cretaceous peralkaline rhyolites (pantellerite and comendite) from Lake Chad, Central Africa. Journal of Geosciences 57, 127–141.
McDonough, W.F., Sun, S.S., 1995. The composition of the Earth. Chemical Geology 120, 223–253.
Meyers, J.B., Rosendahl, B.R., Harrison, C.G.A., Ding, Z.D., 1998. Deep-imaging seismic and gravity results from the offshore Cameroon volcanic line and speculation of African hotlines. Tectonophysics 284, 31–63.
Miyashiro, A., 1978. Nature of alkalic volcanic rock series. Contributions to Mineralogy and Petrology 66, 91–104.
Middlemost, E.A.K., 1975. The basalt clan. Earth-Science Reviews 11, 337–364.
Morimoto, N., 1989. Nomenclature of pyroxenes. Canadian Mineralogist 27, 143–156.
Ngounouno, I., Moreau, C., Déruelle, B., Demaiffe, D., Montigny, R., 2001. Pétrologie du complexe alcalin sous-saturé de Kokoumi (Cameroun). Bulletin de la Société Géologique de France 176, 675–686.
Ngounouno, I., Déruelle, B., Montigny, R., Demaiffe, D., 2005. Petrology and geochemistry of monchiquites from Tchircotché (Garoua rift, north Cameroon, central Africa). Mineralogy and Petrology 83, 167–190.
Ngounouno, I., Déruelle, B., Montigny, R., Demaiffe, D., 2006. Les camptonites du mont Cameroun, Cameroun, Afrique. Comptes Rendus Géoscience 338, 537–544.
Nimis, P., Ulmer, P., 1998. Clinopyroxene geobarometry of magmatic rocks. Part 1: an structural geobarometer for anhydrous and hydrous, basic and ultrabasic systems. Contributions to Mineralogy and Petrology 133, 122–135.
Nkouathio, D.G., Kagou Dongmo, A., Bardintzeff, J.M., Wandji, P., Bellon, H., Pouclet, A., 2008. Evolution of volcanism in graben and horst structures along the Cenozoic Cameroon line (Africa): implications for tectonic evolution and mantle source composition. Contributions to Mineralogy and Petrology 94, 287–303.
Nkoumbou, C., Déruelle, B., Velde, D., 1995. Petrology of Mt Etinde nephelinite series. Journal of Petrology 36, 373–395.
O'Reilly, S.Y., Griffin, W.L., Ryan, C.G., 1991. Residence of trace elements in metasomatized spinel lherzolite xenoliths: a proton-microprobe study. Contributions to Mineralogy and Petrology 109, 98–113.
Palacz, Z.A., Saunders, A.D., 1986. Coupled trace element and isotope enrichment in the Cook–Austral– Samoa islands, southwest Pacific. Earth and Planetary Science Letters 79, 270–280.
Pouchou, J.L., Pichoir, F., 1991. Quantitative analysis of homogeneous or stratified microvolumes applying the model "PAP". In: Heinrich, K.F.J., Newbury, D.E. (Eds.), Electron Probe Quantification. Plenum Press, New York, pp. 31–75.
Roeder, P.L., Emslie, R.F., 1970. Olivine-liquid equilibrium. Contributions to Mineralogy and Petrology 29, 275–289.
Sibuet, J.C., Mascle, J., 1978. Plate kinemetic of Atlantic equatorial fracture zone trends. Journal of Geophysical Research 83, 3401–3421.
Spencer, K.J., Lindsey, D.H., 1981. A solution model for coexisting ion–titanium oxides. American Mineralogist 66, 1189–1201.
Sun, S.S., McDonough, W.F., 1989. Chemical and isotopic systematics of oceanic basalts: implications for mantle composition and processes. In: Saunders, A.D., Norry, M.J. (Eds.), Magmatism in the Ocean Basins, Geological Society of London, Special Publication, 42, pp. 313–345.
Villemant, B., Jaffrezic, H., Joron, J.L., Treuil, M., 1981. Distribution coefficients of major and trace-elements. Fractional crystallization in the alkali basalt series of Chaine des Puys (Massif Central, France). Geochimica et Cosmochimica Acta 45, 1997–2016.
Weaver, B.L., 1991. The origin of ocean island basalt end-member compositions: trace element and isotopic constraints. Earth and Planetary Science Letters 104, 381–397.
Woodland, A.B., Jugo, P.J., 2007. A complex magmatic system beneath the Devès volcanic field, Massif Central, France: evidence from clinopyroxene megacrysts. Contributions to Mineralogy and Petrology 153, 719–773.
Yamgouot, F.N., Déruelle, B., Mbowou, I.B.G., Ngounouno, I., 2015. Petrology of the volcanic rocks from Bioko Island ("Cameroon Hot Line"). International Journal of Geosciences 6, 247–255.
Yokoyama, T., Aka, F.T., Kusakabe, M., Nakamura, E., 2007. Plume-lithosphere interaction beneath Mt. Cameroon volcano, west Africa: constraints from $^{238}U–^{230}Th–^{226}Ra$ and Sr—Nd—Pb isotope systematics. Geochimica et Cosmochimica Acta 71, 1835–1854.
Zindler, A., Hart, S., 1986. Chemical geodynamics. Annual Review of Earth and Planetary Science 14, 493–571.